bioRxiv preprint doi: https://doi.org/10.1101/498261; this version posted December 16, 2018. The copyright holder for this preprint (which was not certified by peer review) is the author/funder, who has granted bioRxiv a license to display the preprint in perpetuity. It is made available under aCC-BY-NC-ND 4.0 International license.

Title: Blood vessels guide Schwann cell migration in the adult demyelinated CNS through Eph/ephrin signaling

Authors and affiliations:

Beatriz Garcia-Diaz*[1,2], Corinne Bachelin[2], Fanny Coulpier[3], Gaspard Gerschenfeld[3], Cyrille Deboux[2], Violetta Zujovic[2], Patrick Charnay[3], Piotr Topilko[3], Anne Baron-Van Evercooren*[2].

[1]Unidad de Gestión Clínica de Neurociencias, IBIMA, Hospital Regional Universitario de Málaga, Universidad de Málaga, Spain.

[2]Institut du Cerveau et de la Moelle Epinière-Groupe Hospitalier Pitié-Salpêtrière, INSERM, U1127, CNRS, UMR 7225, F-75013 Paris; Sorbonne Universités, Université Pierre et Marie Curie Paris 06, UM-75, F-75005 Paris, France.

[3]Ecole normale supérieure, PSL Research University, CNRS, Inserm, Institut de Biologie de l'Ecole normale supérieure (IBENS), F-75005 Paris, France

Conflict of interest : The authors have declared that no conflict of interest exists.

***Corresponding authors**

Beatriz Garcia Diaz, PhD
Brain and Spine Institute (ICM)
ICM Building, 5th floor, 5.031
47 bd de l'Hôpital
Paris 75013
France
Tel : +33 (0)1 57 27 4170
e-mail: beatriz.garcia@icm-institute.org

Anne Baron Van-Evercooren, PhD
Brain and Spine Institute (ICM)
ICM Building, 5th floor, 5.031
47 bd de l'Hôpital
Paris 75013
France
Tel : +33 (0) 01 57 27 41 23
e-mail: anne.baron@upmc.fr

bioRxiv preprint doi: https://doi.org/10.1101/498261; this version posted December 16, 2018. The copyright holder for this preprint (which was not certified by peer review) is the author/funder, who has granted bioRxiv a license to display the preprint in perpetuity. It is made available under aCC-BY-NC-ND 4.0 International license.

ABSTRACT

Schwann cells (SC) enter the central nervous system (CNS) in pathophysiological conditions. However, how SC invade the CNS to remyelinate central axons remains undetermined. We studied SC migratory behavior *ex vivo* and *in vivo* after exogenous transplantation in the demyelinated spinal cord. Data highlight for the first time that SC migrate preferentially along blood vessel in perivascular ECM, avoiding CNS myelin. We demonstrate *in vitro* and *in vivo* that this migration route occurs by virtue of a dual mode of action of Eph/ephrin receptor. Indeed, EphrinB3, enriched in myelin, interacts with SC Eph receptors, to drive SC away from CNS myelin, and triggers their preferential adhesion to ECM components, such as fibronectin via integrinβ1 interactions. This complex interplay enhances SC migration along the blood vessel network and together with lesion-induced vascular remodeling facilitates their timely invasion of the lesion site. These novel findings elucidate the mechanism by which SC invade and contribute to spinal cord repair.

bioRxiv preprint doi: https://doi.org/10.1101/498261; this version posted December 16, 2018. The copyright holder for this preprint (which was not certified by peer review) is the author/funder, who has granted bioRxiv a license to display the preprint in perpetuity. It is made available under aCC-BY-NC-ND 4.0 International license.

INTRODUCTION

Myelination, the evolutionary characteristic acquired by vertebrates to allow rapid and saltatory nerve conduction, is supported by two different glial cell types, oligodendrocytes in the central nervous system (CNS), and Schwann cells (SC) in the peripheral nervous system (PNS). These two cell types are mutually exclusive in physiological conditions. However, in demyelinating diseases or injury, this PNS/CNS segregation is compromised and both, SC can invade and repair the CNS(1, 2), and oligodendrocytes myelinate peripheral nerve root axons(3). Remyelination of CNS axons by SC protects axons, restores axonal conduction and even reverses neurological deficits(4), highlighting their potential to rescue the injured CNS(5). These remyelinating SC arise either from the PNS(6, 7), or are generated from adult oligodendrocyte precursors cells (OPC)(8, 9). However, SC remyelination of CNS axons is always restricted to the spinal roots entry and exit zones (reviewed in(5)),and the presence of peripheral myelin has been frequently observed close to blood vessels (BV)(1). These observations suggest that although SC migrate efficiently *in vitro*(10, 11) and *in vivo*(12) into the PNS, their survival and migration within the CNS are limited. The presence of peripheral myelin close to BV raises the possibility for BV to play a role in guiding SC movements within the CNS. While migration along BVs has been recently described for different CNS cell types(13-15) including for SC along regenerative nerves(12), their role in SC invasion of the CNS has not been explored.

Astrocytes(16, 17) and CNS white matter(18-20) inhibit SC migration within CNS, pointing out that multiple CNS components can alter this process. Among the molecules involved in various cell type segregation and guidance within the CNS, the Eph/ephrin family has been implicated in both developmental(21, 22) and

bioRxiv preprint doi: https://doi.org/10.1101/498261; this version posted December 16, 2018. The copyright holder for this preprint (which was not certified by peer review) is the author/funder, who has granted bioRxiv a license to display the preprint in perpetuity. It is made available under aCC-BY-NC-ND 4.0 International license.

pathological conditions(23). In particular, EphrinB3, is expressed in myelin in brain and mouse spinal cord(24-26), and plays an important role in preventing neurite outgrowth(24), axonal regeneration(25) and oligodendrocyte progenitor differentiation(26). EphrinB3 acts also as a repellent molecule in the guidance of axon tracts towards the spinal cord during development(27). Interestingly, SC express several Ephrin receptors, including EphA4 that mediates SC repulsion by astrocyte EphrinAs(28). Hence, these receptors could mediate also similar SC repulsion by myelin-associated EphrinB3. In addition, EphB is involved in SC sorting and migration in regenerating peripheral nerves(29). Eph/ephrin signalling is involved in the modulation of cell-cell adhesion, which results in increased integrin-mediated adhesion of Eph/ephrin-expressing cells(30, 31) or, as in the case of EphB signaling, in cell sorting by re-localization of N-cadherin in SC(29). Furthermore, EphrinB ligands control cell migration through positive adhesion to substrates such as collagen and fibronectin (FN)(32, 33), main components of perivascular extracellular matrix (ECM). Therefore, these cues could influence the capacity of SC to migrate within the CNS and/or interact with CNS myelin.

In spite of these observations, a role for BV in SC migration/recruitment in the CNS and for EphrinB3 in modulating SC interactions with CNS myelin and/or BV has not been investigated. Using *ex vivo*, *in vivo* and *in vitro* paradigms, we show that BV are a preferred substrate for SC migration into the CNS, and that, angiogenesis and BV remodeling constitute a physiological response to demyelination. Moreover, we establish that CNS myelin plays an essential role in SC exclusion from the CNS and demonstrate that this effect is partially mediated by EphrinB3. Finally, myelin-associated EphrinB3 modulates SC adhesion to the ECM component FN, via interactions with integrinβ1. This increased SC-FN adhesion, to perivascular ECM

bioRxiv preprint doi: https://doi.org/10.1101/498261; this version posted December 16, 2018. The copyright holder for this preprint (which was not certified by peer review) is the author/funder, who has granted bioRxiv a license to display the preprint in perpetuity. It is made available under aCC-BY-NC-ND 4.0 International license.

overrules SC inhibition by myelin and promotes SC migration along BV, facilitating their arrival at the lesion. Thus Eph/ephrin may guide SC within the CNS according to a dual mode, repulsing SC from CNS white matter on one hand, and favoring their interaction with BV on the other. These observations shed new light on the mechanism of SC invasion into the damaged CNS.

bioRxiv preprint doi: https://doi.org/10.1101/498261; this version posted December 16, 2018. The copyright holder for this preprint (which was not certified by peer review) is the author/funder, who has granted bioRxiv a license to display the preprint in perpetuity. It is made available under aCC-BY-NC-ND 4.0 International license.

RESULTS

Schwann cells preferential migration along blood vessels by passes their inhibition by myelin

To address this question, we analysed the SC interactions with CNS components, myelin and blood vessels, in *ex vivo* and *in vivo* paradigms (Fig. 1, Fig. S1 and Fig. S2). For *ex-vivo* analysis, GFP-expressing SC (GFP^+) were seeded on frozen spinal cord sections. We found that GFP^+SC adhered 11.88 fold more over grey matter than white matter (Fig S1A, C). Moreover, SC spreading over white matter was reduced compared to grey matter (Fig. S1D). Immunolabeling for Glut1 showed that BV were 7.78 fold more abundant in grey matter than white matter (Fig. S1B,E) and that most GFP^+ SC (> 86%) were in contact with collagen 4-positive BV (Fig. S1F), indicating that SC densities in grey and white matter were correlated with BV densities in these regions.

To explore how endogenous SC invade the CNS in response to demyelination, we used the Krox20Cre driver line crossed over Rosa-YFP to track the SC lineage(3, 34). Krox20 transcription factor is specific of the PNS, and is expressed in the SC lineage until adulthood. LPC injections were performed in the dorsal funiculus of adult mice (2-3month-old), and mice were sacrificed at 3 days post injection (dpi). YFP^+SC were detected only in the spinal cord cross sections of demyelinated mice (Fig. S2A,B) but not in controls (Fig S2C,D). YFP+ cells were $Sox10^+$ (Fig. S2E,F) but never Olig2+ validating their PNS glial origin. We next examined the location of the invading SC-derived population and found that at this early time-point, the $YFP^{+/}Sox10^+$SC within white mater were found exclusively on $Glut1^+$BV. This indicates that such as observed *ex-vivo,* endogenous SC preferentially associate with

bioRxiv preprint doi: https://doi.org/10.1101/498261; this version posted December 16, 2018. The copyright holder for this preprint (which was not certified by peer review) is the author/funder, who has granted bioRxiv a license to display the preprint in perpetuity. It is made available under aCC-BY-NC-ND 4.0 International license.

BV when triggered to invade the demyelinating CNS. Although in normal development Krox20 specifically labels the peripheral SC lineage, under pathological conditions Krox20 was also expressed by Iba1+ microglial cells (Fig.S2G,H).

As the Krox20Cre system was limited in tracing a sufficient number of SC invading the CNS from the periphery, we pursued our investigation using an exogenous paradigm in which GFP$^+$SC were grafted two vertebrates away from a lysolecithin (LPC) lesion in the dorsal funiculus of adult wild-type mice (Fig 1A). In this paradigm, grafted SC are known to be recruited specifically by the lesion, modeling SC recruitment after CNS injury, whereas they remain at the graft site in the absence of a lesion(20, 35). As our study focused essentially on SC migration/recruitment, grafted animals were sacrificed at early time-points including 1, 3 and 5-day post-LPC injection (dpi) (Fig. 1B). The spatio-temporal distribution of the transplanted GFP-expressing SC was assessed by scanning longitudinal frozen sections of the spinal cord for the GFP signal throughout the sections(20). At 1 dpi, lesion size (0.40 ± 0.06 mm^2 per section) and GFP$^+$SC grafted area (0.16 ± 0.08 mm^2 per section) showed minor variability among animals validating the lesion-graft paradigm. Analysis of the GFP signal over time confirmed the spatio-temporal progression of SC towards the lesion, which was systematically reached at 5 dpi (Fig. 1B,C).

In the intermediate zone connecting the graft to the lesion, GFP$^+$SC migrated preferentially along the midline avoiding myelin (Fig. 1C,D), as previously described after engraftment in shiverer and nude mice(20, 35). In this area, SC were found preferentially in association with Glut1$^+$BV forming a narrow stream of cells (Fig. 1C$_2$,D). At their arrival in the lesion, GFP$^+$SC were no longer confined to that narrow path, but randomly spread within the lesion. Co-detection of GFP and Glut1 at the lesion showed that the pattern of GFP$^+$SC matched with that of Glut1$^+$BV (Fig.

bioRxiv preprint doi: https://doi.org/10.1101/498261; this version posted December 16, 2018. The copyright holder for this preprint (which was not certified by peer review) is the author/funder, who has granted bioRxiv a license to display the preprint in perpetuity. It is made available under aCC-BY-NC-ND 4.0 International license.

1C$_3$).Co-labeling for Glut1 and GFAP showed that GFP$^+$SC were localized in perivascular spaces between endothelial cells and astrocyte end-feet (Fig. 1E). SC within the BV lumen were never observed.

We used whole-mount immuno-labeling of clarified spinal cords to gain insight in SC-BV3D spatial organization. For these experiments, tdTomato$^+$ SC were grafted remotely from the lesion as above, and their migratory behavior analyzed at 5 dpi. BV and SC were visualized by immuno-labeling against anti-IgG and anti-Tomato respectively. Light sheet imaging and 3D reconstruction revealed the dense spinal cord vascular network and confirmed that grafted SC, en route towards the lesion, were preferentially associated with BV in the spinal cord midline (Fig. 1F). TdTomato$^+$ SC were either polarized along blood vessels (Fig. 1G,H,I) or extending processes from one vessel to another (Fig. 1J,K,L).

Whether SC moved along blood vessels was further confirmed by GFP$^+$SC live-imaging2 days post engraftment in the demyelinated spinal cords and host BV were labeled by intra-cardiac perfusion of rhodamine-lectin. Spinal cord whole mounts were maintained in appropriate physiological conditions, and areas containing GFP$^+$SC were selected and video-recorded for 20 hours. Recordings confirmed that SC leaving the graft, reached for and became associated with BV, to migrate either in chains or as isolated cells, jumping from one BV to another one (MovieS1, Fig. S3A, blue empty arrowhead) or sliding along them (MovieS1, Fig. S3A, white arrowhead) as described above. While SC in chains glided along each other, individual cells escaped from the chain crawling along BV outer surface and merging further with other SC (Movie S2, Fig. S3B arrowhead).

bioRxiv preprint doi: https://doi.org/10.1101/498261; this version posted December 16, 2018. The copyright holder for this preprint (which was not certified by peer review) is the author/funder, who has granted bioRxiv a license to display the preprint in perpetuity. It is made available under aCC-BY-NC-ND 4.0 International license.

To elucidate whether SC migrate *in vivo* in association with peri-vascular ECM, and/or whether they require direct interactions with endothelial cells, we performed immuno-electron microscopy (EM) on a novel series of GFP$^+$SC grafted mice (Fig. 1M,N,O). EM analysis of DAB labeled GFP$^+$SC confirmed their location in close contact with BV. Interestingly, the majority of the grafted SC was embedded within the peri-vascular ECM (Fig. 1M,N) between the vascular cells and astrocyte end-feet (Fig. 1O). However, unlike observed in the injured PNS(12), direct contact with vascular cells was never observed.

Temporal analysis of SC arrival at the lesion indicated that in lesions which had cells at early stages (3dpi), 62±9% of GFP$^+$SC were closely associated with BV(Fig. 2A-C,G),while at later times (5dpi) only 32±5% of them were associated with BV (Fig. 2D-F,G). Immunohistochemistry for Glut1 and NF200 indicated that this transition correlated with a change in SC-BV to SC-Axon associations, with only 35±6% of GFP$^+$SC associated with axons at 3dpi (Fig.2A,E,H), and61±5% GFP$^+$SC associated with axons at 5days (Fig. 2B,D,H).

LPC induced demyelination promotes angiogenesis and blood vessel remodeling.

Since angiogenesis has been described in demyelinating diseases(36) and perivascular niche plays a role in remyelination(9), we examined the dynamics of BV in the absence of SC grafting. We found an increase in BV density in lesions of non-grafted spinal cords (Fig. 3B-E), compared to PBS-injected spinal cords (Fig. 3A). Glut1-positivity increased from day 3dpi up to 7dpi with a peak at 5dpi compared to PBS injected controls (Fig. 3I). This transient increase in BV density in LPC lesions was partially due to increased proliferation of endothelial cells based on the number

bioRxiv preprint doi: https://doi.org/10.1101/498261; this version posted December 16, 2018. The copyright holder for this preprint (which was not certified by peer review) is the author/funder, who has granted bioRxiv a license to display the preprint in perpetuity. It is made available under aCC-BY-NC-ND 4.0 International license.

of Glut1^{+}cells, expressing Ki67 (Fig. 3A-F,J, Fig. S4,S5, Supplementary note 1), pointing to an increase of newly formed vessels as a specific reaction to demyelination in addition to BV remodeling. Immuno-labeling for FN and collagen 4 showed that LPC-induced angiogenesis/BV remodeling was concomitant with changes in perivascular ECM (Fig. S6).

We examined whether the presence of exogenous SC could influence the formation of new blood vessels. We found no difference in Glut1^{+}area in lesions of SC-grafted mice compared to lesions of non-grafted ones at 5dpi (Fig. 3G,I). Moreover, no change in Glut1^{+}area was observed at the SC graft site compared to PBS injected mice at 5dpi(Fig. 3H,I).

Myelin-associated EphrinB3 as candidate to guide Schwann cells in the CNS.

Since no effect of exogenous SC on vascularization was observed, we hypothesized that SC guidance within the CNS by SC-BV association and myelin repulsion could be due to some receptor-ligand mediated mechanism. We previously demonstrated that SC are repulsed by CNS myelin, partially mediated by the axonal repellent MAG, suggesting that other myelin components might be involved in this repulsion(20).

Thus, we speculated that other axonal growth inhibitors were able to induce the same effect in SC. Of interest, EphrinB3 is expressed by CNS myelin and inhibits axonal growth and oligodendrocyte differentiation(25, 26), and SC express several EphR(28). Interestingly, Immature stages of the SC lineage such as boundary cap cells and SC precursors, have a greater capacity to migrate through white matter compared to more mature SC stages(37, 38)present lower expression of another EphrinB3 receptor, the EphB6(39). In support of these data, we performed gene profiling by RNA sequencing, comparing aged-matched wild-type and

bioRxiv preprint doi: https://doi.org/10.1101/498261; this version posted December 16, 2018. The copyright holder for this preprint (which was not certified by peer review) is the author/funder, who has granted bioRxiv a license to display the preprint in perpetuity. It is made available under aCC-BY-NC-ND 4.0 International license.

developmentally arrested SC lacking Krox20 (Krox20^{null} SC)(40)(considered at a more immature-like stage) revealed a dysregulation in the transcript levels of a variety of molecules among which Eph receptors were particularly expressed at lower level. While EphA4, EphB1, EphB2, EphB3, EphB4 and EphB6 transcripts were expressed in wild-type SC, EphA4, EphB1 and EphB6 were significantly down-regulated inKrox20^{null} SC (Fig. S7). Hence, we hypothesized that EphA4, EphB6, and EphB1 could be involved in SC poor mingling with CNS white matter, and favorable association with BV.

The EphrinB3 present in myelin is able to bind and activate EphrinB3-receptors in Schwann cells.

We first confirmed that SC have the molecular machinery to bind myelin-associated EphrinB3.Immunohistochemistry showed that purified mouse SC can bind EphrinB3 *in vitro*, and that these cells express the three EphrinB3 receptors: EphB6 (Fig. 4A), EphA4 (Fig. 4C) and EphB1 (Fig. 4D). The presence of each receptor was corroborated by Western blot (Fig. 4B). Incubation of SC with pre-clustered EphrinB3by fluorescent anti-Ig and orthogonal views revealed that the three receptors were able to bind clustered EphrinB3 on SC surface leading to the formation of large signaling clusters as previously described(41) (Fig. 4A,C,D).

Eph receptors are activated by auto-phosphorylation of specific tyrosine residues(42). To verify the ability of EphrinB3 to induce forward signaling, activation of Eph receptors on SC was assessed. Immunocytochemistry illustrates binding of EphA4 with clustered EphrinB3, and its activation by the ligand (Fig. 4E). EphB6 is a recognized Kinase-defective receptor, which can form a hetero-receptor complex with EphB1 receptor and undergoes trans-phosphorylation(43). Immunohistochemistry

bioRxiv preprint doi: https://doi.org/10.1101/498261; this version posted December 16, 2018. The copyright holder for this preprint (which was not certified by peer review) is the author/funder, who has granted bioRxiv a license to display the preprint in perpetuity. It is made available under aCC-BY-NC-ND 4.0 International license.

validated the presence of phospho-Y594 in EphB1 (and EphB2) receptor, and its interaction with bound EphrinB3 in SC (Fig. 4F).

To test the hypothesis that myelin associated EphrinB3 is able to induce the activation of EphB and EphA4 receptors, we incubated purified SC during 30min with myelin protein extracts or myelin protein extract previously incubated with anti-EphrinB3 known to block specifically its activity(26). SC were collected and blotted with an antibody against the phosphorylated EphA4 (Fig. 4G), and an antibody against phosphorylated EphB1+2 (Fig. 4H). The presence of myelin increased significantly the phosphorylated forms of both receptors compared to the housekeeping GAPDH, but this signal increase was not observed when the myelin extracts were pre-incubated with anti-EphrinB3 antibody before activation (Fig.4G,H). Blocking the epitopes of EphrinB3 in myelin neutralized the Eph receptor activation effect of myelin on SC.

Hence, these observations evidenced the ability of SC to bind and respond to the presence of EphrinB3 *in vitro*.

CNS myelin inhibits Schwann cell adhesion and spreading, and this effect is partly mediated by EphrinB3 through EphA4 and EphB6 receptors.

Next, we examined whether EphrinB3 could contribute to SC-myelin repulsion. We performed a blocking receptor assay, pre-incubating purified GFP^{+}SC with unclustered EphrinB3-Fc molecules before seeding them for 3 hours onto myelin protein extract or PBS (Fig.5A), and evaluated both SC adherence and polarization (Fig.5B). Control Fc-preincubated SC showed less adhesion to myelin, measured as the ratio of adhered SC to myelin compared to PBS coated surfaces. SC also extended fewer processes, based on a higher ratio of round cells over the total

bioRxiv preprint doi: https://doi.org/10.1101/498261; this version posted December 16, 2018. The copyright holder for this preprint (which was not certified by peer review) is the author/funder, who has granted bioRxiv a license to display the preprint in perpetuity. It is made available under aCC-BY-NC-ND 4.0 International license.

adhered SC on myelin compared to control. Blocking EphrinB3 receptors on SC by soluble EphrinB3-Fc hindered myelin repulsion, resulting in a significant improvement of SC adhesion to myelin-coated surfaces, and ability to extend more processes (fewer round cells) on myelin than those pre-incubated only with soluble Fc (Fig.5A,B).

To determine if the reduction in the number of SC adhering to myelin was due to cell death, we assessed cell viability comparing the percentage of caspase3^{+} nuclei or Hoechst^{+} pycnotic nucleiin SC incubated with PBS or myelin for 3h.SC exhibited a typical bipolar morphology and no difference in the percentage of caspase3^{+} nuclei or Hoechst pycnotic nuclei between control and myelin-treated groups were observed (PBS: 4.4±1.6‰, Myelin: 4.0±1.7‰, n=6). These data corroborate our previous results demonstrating that short incubation time with myelin does not induce apoptosis(20).

SC adhesion to surfaces coated with EphrinB3-Fc was reduced compared to Fc as control in a dose-dependent manner (Fig. 5C).Moreover, the increased number of round SC indicated that SC were less polarized on EphrinB3 coated surfaces compared to control(significance reached with high concentrations of EphrinB3) (Fig. 5C).

EphrinB3 behaves as a dependence receptor, which can trigger cell apoptosis(44). To analyze the potential effect of EphrinB3 on Schwann cell survival, we assayed cell viability as above. Incubation of adhered SC with clustered EphrinB3, or Fc as controls, for 3h and 24hdid not induce any morphological difference, and the number of H^{+}pycnotic or caspase3^{+}nuclei between Ephrin-treated and control SC remained equivalent (3h treatment (n=6): Fc: 4.4±2‰, EphrinB3: 4.4±2‰; 24h post-treatment (n=8): Fc: 9.7±4‰, EphrinB3: 10.4±3‰). Adhesion assays were always performed in

bioRxiv preprint doi: https://doi.org/10.1101/498261; this version posted December 16, 2018. The copyright holder for this preprint (which was not certified by peer review) is the author/funder, who has granted bioRxiv a license to display the preprint in perpetuity. It is made available under aCC-BY-NC-ND 4.0 International license.

serum-free medium, compromising SC proliferation. These results imply that the reduction in the number of attached and spread SC to the different substrates results from their preferential adhesion rather than a toxic effect of the treatment.

To validate the involvement of EphA4 and EphB6 receptors in SC-EphrinB3 response, we performed the myelin and EphrinB3 adhesion assay in the presence of antibodies that specifically interfere with EphA4 or/and EphB6 receptors, to block SC response. Blocking EphA4 or EphB6 receptor with excess anti-EphA4 or anti-EphB6 respectively improved SC adhesion and spreading to myelin compared to PBS (Fig. 5D) or to EphrinB3 compared to Fc (Fig. 5E). However, no synergistic/additive effect on adhesion was observed when antibodies to both receptors were combined (Myelin/PBS: anti-EphA4 + anti-EphB6: 0.8±0.2(n=11), *p*(IgG vs anti-EphA4 + anti-EphB6)=0.003; EphrinB3/Fc:anti-EphA4 + anti-EphB6: 0.8±0.3(n=10), *p*(IgG vs anti-EphA4 + anti-EphB6)=0.008) two-tailed t-student test.Anti-EphB6 and anti-EphA4 pre-incubation did not show a significant difference in the number of round cells between myelin or EphrinB3 respect to PBS or Fc substrates respectively, and each group respect to the IgG control group.

EphrinB3 increases Schwann cell adhesion and migration on the perivascular ECM component, fibronectin, via integrin ß1

Eph/ephrin can modulate cellular pathways by regulating cell adhesion, either positively or negatively, depending upon the cellular context(45). Thus, positive regulation of SC adhesion to ECM and FN might have consequences on their migration capacity on this substrate(32, 33). As our *in vivo* study indicated that the grafted SC were embedded in perivascular ECM, and angiogenesis is a response to demyelination, we studied the effect of EphrinB3 on SC-ECM binding, in particular FN, that favors SC migration(10). Unlike SC repulsion byEphrinB3-coated surfaces,

bioRxiv preprint doi: https://doi.org/10.1101/498261; this version posted December 16, 2018. The copyright holder for this preprint (which was not certified by peer review) is the author/funder, who has granted bioRxiv a license to display the preprint in perpetuity. It is made available under aCC-BY-NC-ND 4.0 International license.

EphrinB3 improved SC adherence and process expansion on FN coated surfaces compared to those coated with FN and Fc (Fig. 6A).

The main FN-binding receptor on SC is the integrin heterodimer α5β1(46), and the integrin family is involved in the Eph/ephrin response(31, 32). To question whether integrinß1 could mediate the mechanism by which EphrinB3 regulates SC-FN binding, we performed an integrinβ1 interfering assay prior to SC adhesion on FN+EphrinB3 (Fig. 6B,C). Anti-integrinβ1 pre-incubation with a specific blocking antibody(47) consistently prevented the increased SC adhesion to FN+EphrinB3 coated surfaces compared to the FN+Fc coated ones. Moreover, Western blot showed that incubation of SC during 30 min with myelin protein extracts (100µg/mL) increased expression of Integrinβ1and this increase was prevented by pre-incubation of the myelin protein extract with anti-EphrinB3 (Fig.6D, E). This suggests that myelin associated EphrinB3 induced integrinβ1 expression, which is involved in the increased ECM adhesion induced by EphrinB3.

We questioned whether this induced SC adhesion to FN could have some implication in their ability to migrate on FN by using the agarose drop assay(48). SC were seeded on FN in the presence of EphrinB3 or Fc, and their migration when exiting the agarose drop, was followed by time-lapse video-microscopy. Significantly more SC migrated out of the drop when sections were coated with FN+EphrinB3 (Fig.6G) compared to control (Fig. 6F,H). Moreover, based on their maximal distance of migration, SC migrated significantly furtheronFN+EphrinB3 compared to control (Fig. 6I).

Finally, we performed interference experiments to analyze the migratory behavior of SC incubated or not with anti-EphA4 on FN substrate alone or FN+Fc or

bioRxiv preprint doi: https://doi.org/10.1101/498261; this version posted December 16, 2018. The copyright holder for this preprint (which was not certified by peer review) is the author/funder, who has granted bioRxiv a license to display the preprint in perpetuity. It is made available under aCC-BY-NC-ND 4.0 International license.

FN+EphrinB3. Analysis of the migration velocity of single cells traced by video microscopy on FN confirmed that SC migrate significantly faster onFN+EphrinB3substrate, compared to Fc+FN control (Fig. S8). This increased speed was counteracted when SC were pre-incubated with anti-EphA4 compared to control IgG. Moreover, data confirmed that pre-incubation with IgG or anti-EphA4 did not impair SC speed or pattern of migration on FN whether seeded over Fc or EphrinB3 (Fig. S8).

***P*re-treatment with anti-Eph4 promotes Schwann cell to mingle more with myelin *in vivo*, and reduces their interaction with blood vessels.**

In vitro experiments established that EphrinB3 had a dual effect, impairing SC interaction with myelin but improving their interaction with FN via increased integrinß1 expression. Moreover perturbation experiments indicated that anti-EphA4 treatments did not affect SC migratory behavior. To examinewhetherEphrinB3 plays a role in their integration/migration into CNS white matter and/or their interaction with BV *in vivo*, we interfered with EphrinB3 by blocking EphA4, and examined SC interactions with BV and myelin. Since no synergic effect was observed *in vitro* when blocking two different receptors, EphA4 appeared to be the candidate of choice. Pre-incubation of SC with the functional anti-EphA4 blocking antibody prior transplantation as above, disrupted SC interaction with BV (Fig. 7A-C compared to D-E), evaluated by the number of SC-BV association (Fig. 7O), and improved their mingling with myelin along their pathway of migration (Fig. 7G,H vs 7I,J). While 67% of SC was associated with BV in the control group, only 45% did so in the anti-EphA4 treated group (Mann Whitney test, p=0.0003)(Fig.7O). Moreover, for the same graft-lesion distance, lesion size and amount of grafted cells, more GFP^{+}SC were found in the lesion site at 5dpi in animals grafted with IgG treated-SC (Fig. 7C,K,L) compared to those grafted with

bioRxiv preprint doi: https://doi.org/10.1101/498261; this version posted December 16, 2018. The copyright holder for this preprint (which was not certified by peer review) is the author/funder, who has granted bioRxiv a license to display the preprint in perpetuity. It is made available under aCC-BY-NC-ND 4.0 International license.

anti-EphA4 treated SC (Fig. 7E,M,N,P). Thus, anti-EphA4 treatment reduced the capacity of SC to progress efficiently along vessels and/or enhanced their sensitivity to other myelin inhibitors.

bioRxiv preprint doi: https://doi.org/10.1101/498261; this version posted December 16, 2018. The copyright holder for this preprint (which was not certified by peer review) is the author/funder, who has granted bioRxiv a license to display the preprint in perpetuity. It is made available under aCC-BY-NC-ND 4.0 International license.

DISCUSSION

Compelling evidences indicate that SC, whether recruited from the periphery or generated from resident progenitor cells, invade the CNS to remyelinate CNS axons after demyelination(5-9), having an obvious impact on clinical recovery(1, 4). However, in spite of their presence within the CNS, SC intrusion of the CNS is restricted to BV proximal to the PNS, and the mechanisms regulating PNS-CNS transgression after myelin injury, remain elusive. To gain insights into PNS-CNS poor interface, we studied SC behavior when confronted with CNS myelin and BV *ex vivo* and *in vivo* in demyelinating conditions. Using classic, live, 3D imaging as well as electron microscopy, we provide solid evidences that SC use the vascular scaffold to migrate within the adult demyelinated CNS. This phenomenon is doubly modulated by increased angiogenesis and perivascular ECM in response to demyelination, as well as by SC restricted migratory capacity by CNS myelin. In particular, the CNS myelin specific component, EphrinB3, negatively regulates SC adhesion to- and spreading on myelin, while enhancing SC adhesion to perivascular ECM and promoting their migration along them.

Extensive intercellular communication and coordinated interaction between the vascular and nervous systems(49, 50)results in a functional neurovascular unit that contributes to wound healing(12), immune response(51) and embryonic development(52). Recently, a new role in supporting long distance migration of different kinds of cells within the nervous systems was attributed to BV, both in the developing and adult nervous system(13, 14)as well as under pathological conditions(12, 15).So far, despite the increasing number of cells guided by BV, the role of these structures in guiding SC within the CNS to participate in CNS repair was not explored. While SC are known to promote endothelial cell migration and

bioRxiv preprint doi: https://doi.org/10.1101/498261; this version posted December 16, 2018. The copyright holder for this preprint (which was not certified by peer review) is the author/funder, who has granted bioRxiv a license to display the preprint in perpetuity. It is made available under aCC-BY-NC-ND 4.0 International license.

angiogenesis(53) as well as to use BV as scaffold during peripheral nerve regeneration(12), our work demonstrates that this SC-BV interface extends to the CNS and is of relevance to their contribution toCNS repair.

We show that BV are a favorable substrate for exogenous SC and guide them towards demyelinating lesions. BV serve as scaffold for SC as soon as they leave the graft and along their path until arrival at the lesion. Along this path, SC are organized in chains going from one BV to another. At their arrival in the lesion, SC embedded in perivascular ECM become more randomly dispersed and this dispersal faithfully overlaps with BV expansion with time (Fig. 1). This suggests that angiogenesis, a common response to demyelination and inflammation, via expansion of the vascular network and ECM increase, facilitates SC entry sites and dispersal in the lesion. Since SC remyelination has shown to have an impact in the nerve function recovery(4), the clinical impact of angiogenesis in remyelination should not be overlooked.

While associated with BV at their arrival at the lesion at 3dpi, SC detached from BV to contact and align with the demyelinated axons at 5dpi. This change in substrate association may result from signals arising from the axons that trigger their differentiation into more mature SC as a first step to myelin repair. The absence of SC away from their narrow path of migration between the graft and lesion as well as their progressive increase in number in the lesion, point to their specific recruitment by the lesion most likely involving attractant signals yet to be defined. Although most of our observations were performed with exogenous SC, induction of demyelination in Krox20 cre Rosa YFP mice, hints that PNS-derived SC(7) triggered to enter the spinal cord by demyelination, use BV as scaffold to reach the lesion during spontaneous repair. SC are generated also from CNS progenitors in response to

bioRxiv preprint doi: https://doi.org/10.1101/498261; this version posted December 16, 2018. The copyright holder for this preprint (which was not certified by peer review) is the author/funder, who has granted bioRxiv a license to display the preprint in perpetuity. It is made available under aCC-BY-NC-ND 4.0 International license.

demyelination(8),[(9)] opening the possibility that these CNS progenitor-derived SC may also use BV to migrate towards more distant injured sites.

In physiological conditions, the vasculature network, consisting of endothelial cells and pericytes surrounded by ECM, is rather dynamic, and angiogenesis is activated in response to damage(54). As part of this structure, ECM undergoes constant remodeling(55), as also observed in MS and animal models, even before symptoms appear(56). We show that injection of the lipid-toxic agent, LPC, in the absence of grafted SC, induced proliferation of endothelial cells in addition to expansion of the vasculature area. As BV remodeling is known to correlate with a change in ECM, we analyzed this impact in our paradigm. We found a prominent increase in FN and collagen 4 expressions, two main ECM components, which provide excellent substrates for SC migration. FN re-expression also affects directly OPC migration and differentiation and therefore, was proposed as a scaffold required to complete remyelination(57). Likewise, FN promotes SC mobility(10) indicating that the observed changes in ECM composition could stimulate SC migration along BV.

BV also support SC migration in the injured PNS. However, in those circumstances, SC create direct contacts via protrusion with endothelial cells to migrate from one nerve stump to the other or *in vitro* when grown in 3D, suggesting that these protrusions constitute mechanical means to propel SC migration along BV in a tight environment(12). Although we found SC associated with BV along their migrating route, direct contact with endothelial cells or pericytes was never observed. Instead SC were heavily embedded in the perivascular ECM, thus indicating that although SC share similar mechanisms to conquer the injured nervous systems, some differences exist in their mode of migration between CNS and PNS, and BV guidance and perivascular ECM seems to prevail for their migration in the CNS. The observed

bioRxiv preprint doi: https://doi.org/10.1101/498261; this version posted December 16, 2018. The copyright holder for this preprint (which was not certified by peer review) is the author/funder, who has granted bioRxiv a license to display the preprint in perpetuity. It is made available under aCC-BY-NC-ND 4.0 International license.

differences may result from different molecular and cellular environment existing between PNS and CNS, including different degrees of confinement in which SC are placed.

We previously demonstrated that SC avoid and are repelled by myelin(20, 58). Here we confirm these data and show that SC prevented to migrate directly through white matter, are somehow forced to migrate on BV. We showed previously that MAG, a CNS myelin component that prevents axonal regeneration in the CNS, is also inhibitory to SC migration and survival(20). While MAG accounted only partially for the repulsive effect of myelin to SC, our data in the developmentally arrested SC (Krox20^{null}) and those on SC expressing low levels of Krox20(39) hint that the better blending with myelin observed in immature stages of the PNS-linage(37, 38) could be due to the lower expression of Eph receptor profile. We identified EphrinB3 as another myelin component negatively regulating SC in contact with CNS myelin. Like MAG, EphrinB3/EphA4 receptor signaling has been implicated in axon pathfinding(27). This suggest that myelin components exerting their inhibitory effect on axons are not exclusively directed against axons, but extend their inhibition to other neural components such as myelin-competent cells, preventing differentiation of oligodendrocyte progenitors into mature oligodendrocytes(59) as well as SC survival, and migration.

We first proved *in vitro*, that SC-bound EphrinB3 is able to activate by phosphorylation both EphA4 and EphB1, as well as to bind EphB6, which can be also transphosphorylated EphB1(43). Once bound to these receptors, EphrinB3 impairs the adhesion of these cells to myelin proteins, diminishing their process extension onto their substrate. Our *in vitro* data indicate that interfering with both EphB6 and EphA4 do not show additional improvement of this myelin-SC repulsion

bioRxiv preprint doi: https://doi.org/10.1101/498261; this version posted December 16, 2018. The copyright holder for this preprint (which was not certified by peer review) is the author/funder, who has granted bioRxiv a license to display the preprint in perpetuity. It is made available under aCC-BY-NC-ND 4.0 International license.

compared to single interference. Eph receptor signaling is not as straightforward as one receptor binding to one ligand. To trigger efficient activation, Eph receptors must cluster, homotypically (one subtype of Eph receptor) or heterotypically (involving the oligomerization of different Eph receptor subtypes)(41). This lack of synergic effect suggests that the mechanism of Eph/ephrin activation in SC might be mediated by heterotypic recruitment independent of the initial receptor activation.

Ephrin signaling includes not only induced repulsion but also modulates expression of adhesion molecules(29-31). We show that myelin-associated EphrinB3 modulates SC adhesion and migration to ECM, in particular FN, and enhanced integrinβ1 expression, overruling SC inhibition by myelin *in vitro* and promoting their migration along BV to reach the demyelinated lesions *in vivo*. This event occurs in correlation with increased FN expression, among other ECM molecules, during BV remodeling in response to demyelination, suggesting that the increased expression of ECM molecules by BV favours SC-BV interaction and subsequent migration along the vasculature *in vivo*.

Despite the present implication of EphA4 and EphB6 receptors in SC response to myelin, and their contribution to SC migration along CNS BV, the involvement of other Eph receptors in SC migration within the CNS should not be disregarded. To mention, EphB2, also expressed by SC and able to bind myelin-associated EphrinB3, mediates SC-SC interaction through N-cadherin re-localization to organize SC chain migration in the PNS(29). In fact, we observed SC in chains forming bridges going from one BV to another (Fig. 1$C_2$and F, Movie S1), suggesting the possible implication of EphB2 in these events.

In addition, EphA4 is involved in SC-astrocyte repulsion(28). Although the interactions between SC and astrocytes has not been explored in this study, the

bioRxiv preprint doi: https://doi.org/10.1101/498261; this version posted December 16, 2018. The copyright holder for this preprint (which was not certified by peer review) is the author/funder, who has granted bioRxiv a license to display the preprint in perpetuity. It is made available under aCC-BY-NC-ND 4.0 International license.

localization of the grafted SC in the vascular unit between the blood vessel wall and the astrocyte feet, suggests that the repulsion exerted by astrocytes can help confining SC to the perivascular space, and contribute to the mechanism of SC migration along BV. Interfering with EphA4 in SC could have altered this interaction and further allowed the grafted cells to escape from their perivascular path and mingle more with the surrounded white matter parenchyma.

In conclusion, we used multiple ex-vivo, in vivo and in vitro approaches to highlight a novel mechanism of guidance and migration of SC during the early events of CNS repair. We also provide strong evidences that the Eph/ephrin family regulates the complex interactions existing between SC myelin and blood vessels. SC encountering myelin-associated EphrinB3, retract their processes failing to mingle with white matter, and adhere preferentially to BV via activation of Integrinβ1. This dual effect, repulsing SC from CNS myelin and enhancing their attraction to basal lamina, directs their migration along CNS vasculature towards the lesion (Fig.8). Lesions of white matter undergoing the formation and/or reshaping of the vasculature with increased expression of ECM adhesion molecules, in particular FN, further triggers SC mobilization throughout the lesion. While SC invasion of the CNS is not restricted to demyelinating diseases, future studies should indicate whether such mechanisms are of relevance for other clinical pathologies such as trauma as well as genetic and acquired myelinopathies.

bioRxiv preprint doi: https://doi.org/10.1101/498261; this version posted December 16, 2018. The copyright holder for this preprint (which was not certified by peer review) is the author/funder, who has granted bioRxiv a license to display the preprint in perpetuity. It is made available under aCC-BY-NC-ND 4.0 International license.

MATERIAL and METHODS

Animals. Eight week old C57Bl/6JR female mice were purchased from Janvier Labs (Rodent Research Models & Associated Services). Actin-green fluorescent protein (GFP) transgenic,*Krox20*$^{Cre/+}$ *R26R*$^{YFP/+(34)}$, and *Krox20*$^{Cre/flox}$,*R26*$^{mT/+(3)}$mice were previously characterized(3, 34), and maintained at ICM and IBENS animal facilities. Animal experiments were performed according to European Community regulations, ICM and INSERM ethical committee (authorization 75-348; 20/04/2005) and were approved by the local Darwin ethical committee.

Schwann cell isolation and purification. Sciatic nerves of wild-type and Tg mice were isolated at postnatal day 15 and purification procedure was adapted from the previously described protocol(35). Briefly, enzymatic dissociation was performed by incubation with trypsin 0.025% and collagenase (420 U/ml) 10min at 37°C, followed by mechanical dissociation through different needle gages. After ending dissociation with fetal calf serum (FCS), SC were seeded in FN-coated flasks, and expanded in Dulbecco's modified Eagles medium, containing 10% heat-inactivated FCS serum, penicillin (100 mg/ml), streptomycin (100 U/ml), human recombinant Neu-differentiation factor ß (hrNDFß) (125 ng/ml), insulin (10 µg/ml) and forskolin (2 µg/ml).SC were purified by differential adhesion(60), obtaining a purity of 90%, and passaged no more than three times before use. Purification was controlled by immunocytochemistry for p75.For adhesion, migration and blocking receptor assays, SC were maintained in Sato serum-free medium(61) supplemented with hrNDFB (125 ng/ml), and forskolin (2 µg/ml).

iDISCO whole-mount immunofluorescence and imaging. Spinal cords were processed as described in the iDISCO protocol(62), including modifications described in the updated online protocol (https://idisco.info, December 2016). The primary

bioRxiv preprint doi: https://doi.org/10.1101/498261; this version posted December 16, 2018. The copyright holder for this preprint (which was not certified by peer review) is the author/funder, who has granted bioRxiv a license to display the preprint in perpetuity. It is made available under aCC-BY-NC-ND 4.0 International license.

antibody used was rabbit anti-RFP (1:1000, Rockland). Secondary antibodies used were donkey anti-rabbit Cy3 (1:800, Jackson Immunoresearch) and donkey anti-mouse IgG Cy5 (1:800, Jackson Immunoresearch) for intravascular staining. The cleared samples were imaged with a light sheet microscope (Ultramicroscope II; LaVision Biotec).

RNA transcriptome analysis. Library preparation and Illumina sequencing were performed at the EBENS genomic core facility. Briefly, (polyA+) mRNAs were purified from 250 ng of total RNA using oligo(dT). Libraries were prepared using the strand specific RNA-Seq library preparation TruSeq Stranded mRNA kit (Illumina). Libraries were multiplexed by 6 on 1 high-output flow cells. A 75 bp read sequencing was performed on a NextSeq 500 device (Illumina). A mean of 94 ± 9,5 million passing Illumina quality filter reads was obtained for each of the 6 samples.

The analyses were performed using the Eoulsan pipeline(63), including read filtering, mapping, alignment filtering, read quantification, normalization and differential analysis. Before mapping, poly N read tails were trimmed, reads ≤40 bases were removed, and reads with quality mean ≤30 were discarded. Reads were then aligned against the Mus musculus genome from Ensembl version 84 using STAR(64). Alignments from reads matching more than once on the reference genome were removed using Java version of SamTools(65). To compute gene expression, Mus musculus GFF3 genome annotation version 84 from Ensembl database was used. All overlapping regions between alignments and referenced gene were counted using HTSeq-count 0.5.3(66). The sample counts were normalized using DESeq 1.8.3(67). Statistical treatments and differential analyses were also performed using DESeq 1.8.3.

bioRxiv preprint doi: https://doi.org/10.1101/498261; this version posted December 16, 2018. The copyright holder for this preprint (which was not certified by peer review) is the author/funder, who has granted bioRxiv a license to display the preprint in perpetuity. It is made available under aCC-BY-NC-ND 4.0 International license.

Data availability. The RNASeq gene expression data and raw fastq files are available on the GEO repository (www.ncbi.nlm.nih.gov/geo/) under accession number: GSE107401 (accession password: mlkfkwoezxujvsn).

Myelin Protein Extract isolation. Myelin was purified by sucrose gradient centrifugation(68). Cerebral hemispheres of adult mice (3 months-old)were homogenized (on ice) in 0.35 M sucrose and 5 mM EGTA and the suspension was overlaid onto an equivalent volume of 0.85 M sucrose and 5 mM EGTA and centrifuged at 100000 x g at 4ºC for 20 min. The myelin-containing fraction at the interface was collected, diluted three-fold in distilled water, and centrifuged at 100000 x g at 4ºC for 30 min. After washing with distilled water, the isolated myelin pellet was re-suspended in 20 mMTris-HCl, aliquoted, and stored at –20ºC.

Pre-clustering of recombinant EphrinB3-Fc. Mouse EphrinB3-Fc fragments and human Fc were purchased by R&D Systems. The soluble forms of EphrinB3-Fc, and its control Fc, have low effect on receptor activation(69), therefore they were mixed with anti-mouse Fc-IgG and anti-human Fc-IgG (Alexa 555) respectively, (ratio = 1:5), and incubated for 1 h at 37°C prior to addition to SC(70).

Adhesion and Spreading Assays.

In vitro. Adhesion and spreading assays were performed in 24 well dishes. Silicon strips on coverslips were used to separate two coated areas of each coverslips(71). Surfaces were coated overnight at 37°C with recombinant EphrinB3-Fc fusion at 10 µg/mL and Fc equimolar (as control) on each side respectively; or myelin extract (100 µg/mL) and PBS buffer, as control. Before cell seeding, strips were removed and coverslips were washed carefully with PBS. 10^5SCwere seeded in serum-free Sato

bioRxiv preprint doi: https://doi.org/10.1101/498261; this version posted December 16, 2018. The copyright holder for this preprint (which was not certified by peer review) is the author/funder, who has granted bioRxiv a license to display the preprint in perpetuity. It is made available under aCC-BY-NC-ND 4.0 International license.

medium to avoid proliferation, and allowed to adhere for 3h. Data were always expressed as ratio respect to the intra-coverslip control(24).

Spinal cord frozensections. Cryostat longitudinal sections(20µm thick)of snap frozen spinal cords were allowed to adhere to glass slides and were thawed at room temperature just before use. Then, 50.000 SC/sections were seeded and allowed to adhere overnight (16h) before fixation in 4% paraformaldehyde (5 min), immunostaining for Glut1and mounting with fluoromount.

Survival assay. GFP^{+}SC were seeded on uncoated glass coverslips in normal medium. After overnight adhesion, medium was changed adding Sato serum-free medium supplemented with clustered-EphrinB3 at 10 µg/mL and Fc equimolar (as control); or myelin extract (100 µg/mL) and PBS (as control). SC were incubated for 3 h or 24 h as specified in each experiment. After fixation in 4% paraformaldehyde (5 min), SC were immuno-stained for caspase 3 adding Hoechst dye to visualize all nuclei, and coverslips mounted with fluoromount.

Migration assay.SC were re-suspended at $3{\cdot}10^{6}$ cells/ml in Sato medium containing 0.8% low melting point agarose (Sigma). 1.5 µL-drops of this suspension were applied to the center of FN +EphrinB3, or FN +Fc-coated glass coverslips, which were placed at 4°C for 1 min to allow the agarose to solidify. The cooled drop was covered with Sato medium with hrNDFß(125 ng/ml) and forskolin (2 µg/ml) and placed up to 6 h at 37 °C into the incubating chamber of a video-microscopy (ZEISS).

SC receptor blocking assay. EphA4 and EphB6 receptors, or Integrinβ1 in SC were neutralized by incubation with anti-EphA4 (1.2 µg/10.000 cells, R&D, AF641), anti-EphB6 (1.2 µg/10.000 cells, Santa Cruz Biotechnology, sc-7282), anti-integrinβ1 (0.6

bioRxiv preprint doi: https://doi.org/10.1101/498261; this version posted December 16, 2018. The copyright holder for this preprint (which was not certified by peer review) is the author/funder, who has granted bioRxiv a license to display the preprint in perpetuity. It is made available under aCC-BY-NC-ND 4.0 International license.

µg/10.000 cells, MA2910, Thermo Fisher Scientific)antibodies or IgG (as control) in Sato medium for 1 h at 37°C prior to cell seeding or transplantation.

Immuno-staining. Cultured SC were fixed for 5 min in 4% paraformaldehyde prior immuno-staining and mice were sacrificed by trans-cardiac perfusion of PBS followed by cold 4% paraformaldehyde, and post-fixed in the same fixative for 1 hour. Spinal cords were cryo-protected by immersion in 20% sucrose solution overnight, embedded in cryomatrix (Thermo Scientific), and frozen in cold isopentane at –60°C. Finally, they were sectioned with a cryostat at 12 µm (Leica Microsystems). Both cells and sections were washed, blocked in 5% BSA for 40 min and incubated with the primary antibodies. While cells were incubated 1h at room temperature, slides were incubated overnight at 4°C. For MOG staining, sections were incubated with absolute ethanol for 10 min followed by primary antibody, and then washed profusely. Primary antibodies were as follows: antiEphA4 (1:50, R&D, AF641); anti-EphA4-Tyr(602) (1:50, ECM Biosciences, EP2731); anti-EphB6 (1:50, SAB4503476, Sigma); anti-EphB1 (1:50, SAB4500776, Sigma; anti-Eph receptor B1+Eph receptor B2 (phospho Y594) (1:50, ab61791, Abcam); anti-Ki67 (1:100, 556003, BD Biosciences); anti-cleaved caspase3 (1:500, Cell Signalling, #9661S); anti-GFP (1:400, Aves, GFP-1020); anti-MOG (1:20, mouse IgG1 hybridoma, clone C18C5; provided by C. Linnington, University of Glasgow, Glasgow, United Kingdom); anti-MBP (1:50, ab7349, Sigma), anti-Glut1 (1:100, 07-1401, Merck Millipore; and 1:400, MABS132, Sigma); anti-Fibronectin (1:600, F6140, Sigma); anti-CD31 (1:200, 553370, BD Pharmigen); anti-NF200 (1:200, N4142,Sigma), anti-p75 (1:100, Ozyme, 8238S), anti-CD13 (1:50, BioRad, MCA2183), anti-CD68 (1:400, BioRad, MCA1957), anti-CD11b (1:400, BioRad, MCA74G), anti-F8/40 (1:100, BioRad, MCA497R), anti-Collagen 4(1:400, ab19808, Abcam), anti-Olig2 (1:300, MABN50, Millipore) and anti-

bioRxiv preprint doi: https://doi.org/10.1101/498261; this version posted December 16, 2018. The copyright holder for this preprint (which was not certified by peer review) is the author/funder, who has granted bioRxiv a license to display the preprint in perpetuity. It is made available under aCC-BY-NC-ND 4.0 International license.

sox10 (1:50, AF2864, R&D System).Next, cells or sections were washed and incubated with secondary antibodies and Hoechst dye for 1h at room temperature. The excess secondary antibody was removed by several PBS washes, and coverslips/slides were mounted using fluoromount.

Electron microscopy. For electron microscopy, mice were perfused with PBS followed by 4% paraformaldehyde/2.5% glutaraldehyde (Electron Microscopy Science) in PBS for 45 minutes. Dissected spinal cords were post-fixed with the same solution for 2 hours, then,sectioned into 60µm slices with a vibratome and washed twice with PBS before enzyme immuno-labeling revealed by DAB/oxygen peroxyde. For DAB revelation, endogenous peroxidase was inhibited with a methanol/oxygen peroxide incubation, washed and blocked by 5% BSA for 1h. Sections were incubated with anti-GFP overnight at 4°C, then washed and incubated with a secondary biotinylated antibody for 2h at room temperature. After several washes with PB 0.1M sections were incubated with the ABC kit (VECTASTAIN® ABC-HRP Kit, Vector Lab) containing peroxidase-antiperoxidase for 40min followed by a DAB/ oxygen peroxide mix before stopping the reaction with distilled water. Samples were fixed in 2% osmium tetroxide (Sigma-Aldrich) 30min, washed gently and incubated with 5% uranyl acetate for 30min in the dark. After dehydration, samples were embedded in Epon resin 812.Ultra-thin sections (80 nm) were examinedwith a HITACHI 120 kV HT-7700 electron microscope.

Demyelinating lesions and grafts. Wild-type mice were anaesthetized with a ketamine/xylazine mixture. Demyelination was induced by stereotaxic injection of LPC (1%, 0.5 µl) in PBS. LPC or PBS (in control animals) was injected into the dorsal funiculus of the spinal cord at the level of T8–T9 in the dorsal column white matter

bioRxiv preprint doi: https://doi.org/10.1101/498261; this version posted December 16, 2018. The copyright holder for this preprint (which was not certified by peer review) is the author/funder, who has granted bioRxiv a license to display the preprint in perpetuity. It is made available under aCC-BY-NC-ND 4.0 International license.

using a glass micropipette. SC (10^5/ 2µL) were injected the same day two vertebrate caudally (4mm) in the same tract.

Western blotting. SC ($6{\cdot}10^6$ cells/well) were lysed in RIPA buffer with Complete® and Phosphostop® inhibitor and analyzed by electrophoresis in an SDS 4–20% MINI PROTEAN TGX gel. After electrophoresis, proteins were transferred electrophoretically to polyvinylidene difluoride membranes and probed with the following antibodies:anti-EphB6 (1:500, SAB4503476, Sigma), anti-EphB1 (1:500, SAB4500776, Sigma), anti-EphA4 (4µg/mL, 37-1600, ThermoFisher), anti-p-EphB1+2 (1:300, ab61791, Abcam), anti-p-EphA4 (1:300, EP2731, ECMBiosciences), anti-Integrinβ1 (1:500, 550531, BD Pharmingen), anti-EphrinB3 (1:250, 1µg/mL, AF395 R&D systems), anti-MBP (1:1000, ab980, Millipore), anti-GAPDH (1:5000, MAB374, Millipore) and anti-Actin (1:50000, A2228, Sigma). Peroxidase-conjugated anti-rabbit, anti-goat or anti-mouse IgG secondary antibodies (Jackson ImmunoResearch) were used at a dilution of 1:5000, 1:10000 and 1:20000, respectively, and anti-Rat biotinylated (1:100, Vector Labs) followed by peroxidase-conjugated streptavidin. Protein bands were visualized by chemoluminescence (ECL BioRad). Intensity of the bands was quantified with ImageJ.

Neutralization of EphrinB3 epitopes in myelin extracts. EphrinB3 epitopes in myelin extract proteins were neutralized by incubation with anti-EphrinB3 antibodies (AF395, R&D system and sc-271328, Santa Cruz Biotechnology; ratio: 1:1) for 2 h at room temperature prior to the addition to the cells(26).

Spinal cord live imaging. LPC lesion followed by GFP+SC engraftment was performed in 60 days-old animals and mice terminally anesthetized. Rhodamine labeled BSL I (Vector Labs RL-1102) at 2mg/ml was injected in the beating heart to label BV. After 5 minutes allowing dye circulation, spinal cords were dissected in ice-

bioRxiv preprint doi: https://doi.org/10.1101/498261; this version posted December 16, 2018. The copyright holder for this preprint (which was not certified by peer review) is the author/funder, who has granted bioRxiv a license to display the preprint in perpetuity. It is made available under aCC-BY-NC-ND 4.0 International license.

cold HBSS solution supplemented with 6,4 mg/mL d-(+)-glucose and bubbled for 30 min with bubbled with 95% O_2/5% CO_2. Spinal cord segments including lesion and graft sites were laid onto Millicell-CM slice culture inserts (Millipore) over culture medium (50% DMEM+Glutamax, 25% HBSS, 25% heat-inactivated horse serum, 5 mg/mL d-(+)-glucose, 20mM Hepes, penicillin (100 mg/ml), streptomycin (100 U/ml), human recombinant neu-differentiation factor ß (hrNDFß) (125 ng/ml), and forskolin (2 µg/ml)in a glass bottom plates, and then placed into an inverted Leica SP8X confocal with an on-stage incubator (while streaming 95% O_2, 5% CO_2 into the chamber). Spinal cords were imaged using a 25x immersion objective at intervals of 15 min during 12 hours with intermittent repositioning of the focal planes. Maximum intensity projections of the collected stacks (~60 µm at 2 µm step size) were compiled in FIJI program.

Quantification

Lesion. The lesion area was identified by immune detection of GFAP combined with Hoechst (H^+) labeled nuclei to reveal astrocyte reactivity and hyper-cellularity respectively.

SC adhesion and spreading in vitro. SC adhesion on different surfaces was quantified as the ratio of the number of adhered GFP^+ on myelin- or EphrinB3-coated areas, over those adhered to uncoated or Fc-coated area within the same coverslip. All coated areas were of equal size. Schwann cell spreading was evaluated by quantifying the ratio of GFP^+SC not able to expand their processes out of the total on myelin- or EphrinB3-coated areas over those on non-coated or Fc-coated.

*SC spreading and adhesion to BV ex vivo.*SC spreading on frozen spinal cord sections was evaluated by quantifying the GFP^+ area per cell identified by $Hoechst^+$

bioRxiv preprint doi: https://doi.org/10.1101/498261; this version posted December 16, 2018. The copyright holder for this preprint (which was not certified by peer review) is the author/funder, who has granted bioRxiv a license to display the preprint in perpetuity. It is made available under aCC-BY-NC-ND 4.0 International license.

nuclei. Adhesion on these sections was evaluated as the number of cells in contact with collagen 4-positive blood vessels.

SC extent of migration in vitro. SC migration was quantified by measuring the number of SC outside the 1.5 µL agarose drop and the maximum extent of their migration from the edge drop.

SC velocity in vitro. SC speed of migration was quantified by manual cell tracking plugging of FIJI program, calibrating pixel size and duration of time-lapse of each frame.

Size of lesion and graft area. Lesion and grafted cells within the dorsal funiculus were quantified by delimiting Hoechst+ nuclei hyperdensity and GFAP-positive areaper12µm-section. Lesion and graft areas were quantified by ImageJ 1.49s. For each animal, at least three serial sections with 60 µm intervals were quantified.

Extent of SC migration in vivo. SC migration within the dorsal funiculus was quantified on longitudinal sections evaluating the distance between the graft injection site and the most proximal GFP^+ cell to the lesion (LPC injection site) in each animal from different groups.

BV expansion. BV were identified by immunoreactivity to Glut1, a marker restricted to micro-vessels with blood-tissue barrier function.BV expansion was quantified as the $Glut1^+$area over a cut-off threshold of staining using ImageJ 1.49s.$Glut1^+$area in controls was averaged and every animal value of both groups was expressed as a ratio over this control mean. Endothelial cell proliferation was assessed taking into account only $Glut1^+$ cells containing a $Ki67^+$ nucleus clearly embedded within their cytoplasm, and excluding $Ki67^+$ nuclei, closely apposed.

bioRxiv preprint doi: https://doi.org/10.1101/498261; this version posted December 16, 2018. The copyright holder for this preprint (which was not certified by peer review) is the author/funder, who has granted bioRxiv a license to display the preprint in perpetuity. It is made available under aCC-BY-NC-ND 4.0 International license.

SC-BV association. SC-BV association was quantified in the intermediate zone, at1mm from the graft edge in the direction of the lesion or in the lesion site. GFP^+/$Hoechst^+$SC, with complete or more than half-cell size in contact with $Glut1^+$ endothelial cells were counted as "closely associated cells" while those with only "tip" contacts or no contacts were considered as "not associated cells". Data are expressed as the percentage of total counted cells in both groups.

SC-Axon alignment. SC-BV alignment in the lesion site was quantified. GFP^+/$Hoechst^+$ SC, with complete or more than half-cell in parallel orientation and aligned closely to $NF200^+$ axons (excluding alignment to BV), were counted as "closely associated cells" while those with only "tip" contacts or no contacts were considered as "not associated cells". Data are expressed as the percentage of total counted cells in both groups.

Statistics

The sample size calculation was performed by the resource equation method, trying to minimize the sample size to follow the ARRIVE guidelines for reporting animal research. Each n represents one animal or SC sample in the experiment. The grafting experiments were repeated at least three times with different set of animals each. For the *in vitro* analysis, experiments were performed at least three times with SC obtained from different dissections and dissociations. Statistical analysis was carried out using GraphPad Prism 6 software. All values were expressed as mean ± SD. Normality in the variable distributions was assessed by the D'Agostino&Pearson omnibus test and Grubbs' test was used to detect and exclude possible outliers. When Normality test was passed, means were compared by two-tailed Student's t test. When one or both groups did not follow a normal distribution, means were compared by two-tailed Mann-Whitney U test. When different independent groups

bioRxiv preprint doi: https://doi.org/10.1101/498261; this version posted December 16, 2018. The copyright holder for this preprint (which was not certified by peer review) is the author/funder, who has granted bioRxiv a license to display the preprint in perpetuity. It is made available under aCC-BY-NC-ND 4.0 International license.

were compared, we performed a one-way ANOVA plus Tukey's multiple comparison tests. One sample t-test was used to compare values to the hypothetical mean: 1 for ratios and 100 for percentages. Repeated-measure ANOVA was used to analyze the difference along time of a certain parameter. P-values lower than 0.05 were used as a cut-off for statistical significance.

Author contributions

B.G-D. coordinated and designed the study, performed most of the experimental work, analyzed and interpreted the results, and wrote the manuscript with critical input from all authors; C.B. performed the *ex vivo* immunohistochemistry experiments; F.C. carried out gene profiling and analysis; G.G. performed iDisco and LightSheet analysis; C.D. assisted with animal experiments; V.Z., P.T., and P.C. critically reviewed the manuscript; A.B-V. conceived the project, handled the funding, supervised and interpreted the results, wrote and edited the manuscript. All of the authors approved the manuscript.

Acknowledgments

The authors thank the ICM and IBENS animal, genomic and cellular imaging core facilities, and the ICM histology core facility for technical assistance. The IBENS Imaging facility received the support of grants from the "Région Ile-de- France" (NERF N°2011-45), the "Fondation pour la Recherche Médicale" (N° DGE 20111123023), and the "Fédération pour la Recherche sur le Cerveau - Rotary International France"(2011).The ICM core facility received funding from the ICM Foundation.

Funding was provided by grants from the National Multiple Sclerosis Society (NMSS), to A.B. and P.C.(RG 5088-A- 1); INSERM, CNRS, ARSEP, and the program

bioRxiv preprint doi: https://doi.org/10.1101/498261; this version posted December 16, 2018. The copyright holder for this preprint (which was not certified by peer review) is the author/funder, who has granted bioRxiv a license to display the preprint in perpetuity. It is made available under aCC-BY-NC-ND 4.0 International license.

“Investissements d’Avenir” (ANR-10- IAIHU-06 and ANR-11- INBS-0011–NeurATRIS) to AB,; INSERM, CNRS, IBENS, the program “Investissements d’Avenir” (ANR-10- IAIHU-06 and ANR-11-INBS- 0011–NeurATRIS) to P.C; the France Génomique national infrastructure, funded as part of the "Investissements d'Avenir" program (contract ANR-10-INBS-09)to P.T the Seventh Framework Programme of the European Union (under the agreement Num. 291730) to B.G-D.

bioRxiv preprint doi: https://doi.org/10.1101/498261; this version posted December 16, 2018. The copyright holder for this preprint (which was not certified by peer review) is the author/funder, who has granted bioRxiv a license to display the preprint in perpetuity. It is made available under aCC-BY-NC-ND 4.0 International license.

REFERENCES

1. Duncan ID, and Hoffman RL. Schwann cell invasion of the central nervous system of the myelin mutants. *J Anat.* 1997;190 (Pt 1)(35-49.
2. Guest JD, Hiester ED, and Bunge RP. Demyelination and Schwann cell responses adjacent to injury epicenter cavities following chronic human spinal cord injury. *Exp Neurol.* 2005;192(2):384-93.
3. Coulpier F, Decker L, Funalot B, Vallat JM, Garcia-Bragado F, Charnay P, and Topilko P. CNS/PNS boundary transgression by central glia in the absence of Schwann cells or Krox20/Egr2 function. *The Journal of neuroscience : the official journal of the Society for Neuroscience.* 2010;30(17):5958-67.
4. Felts PA, and Smith KJ. Conduction properties of central nerve fibers remyelinated by Schwann cells. *Brain research.* 1992;574(1-2):178-92.
5. Zujovic V, Bachelin C, and Baron-Van Evercooren A. Remyelination of the central nervous system: a valuable contribution from the periphery. *Neuroscientist.* 2007;13(4):383-91.
6. Assinck P, Duncan GJ, Plemel JR, Lee MJ, Stratton JA, Manesh SB, Liu J, Ramer LM, Kang SH, Bergles DE, et al. Myelinogenic Plasticity of Oligodendrocyte Precursor Cells following Spinal Cord Contusion Injury. *The Journal of neuroscience : the official journal of the Society for Neuroscience.* 2017;37(36):8635-54.
7. Ma D, Wang B, Zawadzka M, Gonzalez G, Wu Z, Yu B, Rawlins EL, Franklin RJM, and Zhao C. A Subpopulation of Foxj1-Expressing, Nonmyelinating Schwann Cells of the Peripheral Nervous System Contribute to Schwann Cell Remyelination in the Central Nervous System. *The Journal of neuroscience : the official journal of the Society for Neuroscience.* 2018;38(43):9228-39.
8. Zawadzka M, Rivers LE, Fancy SP, Zhao C, Tripathi R, Jamen F, Young K, Goncharevich A, Pohl H, Rizzi M, et al. CNS-resident glial progenitor/stem cells produce Schwann cells as well as oligodendrocytes during repair of CNS demyelination. *Cell stem cell.* 2010;6(6):578-90.
9. Ulanska-Poutanen J, Mieczkowski J, Zhao C, Konarzewska K, Kaza B, Pohl HB, Bugajski L, Kaminska B, Franklin RJ, and Zawadzka M. Injury-induced perivascular niche supports alternative differentiation of adult rodent CNS progenitor cells. *eLife.* 2018;7(
10. Baron-Van Evercooren A, Kleinman HK, Seppa HE, Rentier B, and Dubois-Dalcq M. Fibronectin promotes rat Schwann cell growth and motility. *The Journal of cell biology.* 1982;93(1):211-6.
11. Milner R, Wilby M, Nishimura S, Boylen K, Edwards G, Fawcett J, Streuli C, Pytela R, and ffrench-Constant C. Division of labor of Schwann cell integrins during migration on peripheral nerve extracellular matrix ligands. *Dev Biol.* 1997;185(2):215-28.
12. Cattin AL, Burden JJ, Van Emmenis L, Mackenzie FE, Hoving JJ, Garcia Calavia N, Guo Y, McLaughlin M, Rosenberg LH, Quereda V, et al. Macrophage-Induced Blood Vessels Guide Schwann Cell-Mediated Regeneration of Peripheral Nerves. *Cell.* 2015;162(5):1127-39.
13. Tsai HH, Niu J, Munji R, Davalos D, Chang J, Zhang H, Tien AC, Kuo CJ, Chan JR, Daneman R, et al. Oligodendrocyte precursors migrate along vasculature in the developing nervous system. *Science.* 2016;351(6271):379-84.
14. Bovetti S, Hsieh YC, Bovolin P, Perroteau I, Kazunori T, and Puche AC. Blood vessels form a scaffold for neuroblast migration in the adult olfactory bulb. *The Journal of neuroscience : the official journal of the Society for Neuroscience.* 2007;27(22):5976-80.
15. Fujioka T, Kaneko N, Ajioka I, Nakaguchi K, Omata T, Ohba H, Fassler R, Garcia-Verdugo JM, Sekiguchi K, Matsukawa N, et al. beta1 integrin signaling promotes neuronal migration along vascular scaffolds in the post-stroke brain. *EBioMedicine.* 2017;16(195-203.
16. Franklin RJ, and Blakemore WF. Requirements for Schwann cell migration within CNS environments: a viewpoint. *International journal of developmental neuroscience : the official journal of the International Society for Developmental Neuroscience.* 1993;11(5):641-9.

bioRxiv preprint doi: https://doi.org/10.1101/498261; this version posted December 16, 2018. The copyright holder for this preprint (which was not certified by peer review) is the author/funder, who has granted bioRxiv a license to display the preprint in perpetuity. It is made available under aCC-BY-NC-ND 4.0 International license.

17. Lakatos A, Barnett SC, and Franklin RJ. Olfactory ensheathing cells induce less host astrocyte response and chondroitin sulphate proteoglycan expression than Schwann cells following transplantation into adult CNS white matter. *Experimental neurology.* 2003;184(1):237-46.
18. Baron-Van Evercooren A, Avellana-Adalid V, Ben Younes-Chennoufi A, Gansmuller A, Nait-Oumesmar B, and Vignais L. Cell-cell interactions during the migration of myelin-forming cells transplanted in the demyelinated spinal cord. *Glia.* 1996;16(2):147-64.
19. Iwashita Y, and Blakemore WF. Areas of demyelination do not attract significant numbers of schwann cells transplanted into normal white matter. *Glia.* 2000;31(3):232-40.
20. Chaudhry N, Bachelin C, Zujovic V, Hilaire M, Baldwin KT, Follis RM, Giger R, Carter BD, Baron-Van Evercooren A, and Filbin MT. Myelin-Associated Glycoprotein Inhibits Schwann Cell Migration and Induces Their Death. *The Journal of neuroscience : the official journal of the Society for Neuroscience.* 2017;37(24):5885-99.
21. Todd KL, Baker KL, Eastman MB, Kolling FW, Trausch AG, Nelson CE, and Conover JC. EphA4 Regulates Neuroblast and Astrocyte Organization in a Neurogenic Niche. *The Journal of neuroscience : the official journal of the Society for Neuroscience.* 2017;37(12):3331-41.
22. Linneberg C, Harboe M, and Laursen LS. Axo-Glia Interaction Preceding CNS Myelination Is Regulated by Bidirectional Eph-Ephrin Signaling. *ASN neuro.* 2015;7(5).
23. Nikolakopoulou AM, Koeppen J, Garcia M, Leish J, Obenaus A, and Ethell IM. Astrocytic Ephrin-B1 Regulates Synapse Remodeling Following Traumatic Brain Injury. *ASN neuro.* 2016;8(1):1-18.
24. Benson MD, Romero MI, Lush ME, Lu QR, Henkemeyer M, and Parada LF. Ephrin-B3 is a myelin-based inhibitor of neurite outgrowth. *Proc Natl Acad Sci U S A.* 2005;102(30):10694-9.
25. Duffy P, Wang X, Siegel CS, Tu N, Henkemeyer M, Cafferty WB, and Strittmatter SM. Myelin-derived ephrinB3 restricts axonal regeneration and recovery after adult CNS injury. *Proceedings of the National Academy of Sciences of the United States of America.* 2012;109(13):5063-8.
26. Syed YA, Zhao C, Mahad D, Mobius W, Altmann F, Foss F, Gonzalez GA, Senturk A, Acker-Palmer A, Lubec G, et al. Antibody-mediated neutralization of myelin-associated EphrinB3 accelerates CNS remyelination. *Acta neuropathologica.* 2016;131(2):281-98.
27. Paixao S, Balijepalli A, Serradj N, Niu J, Luo W, Martin JH, and Klein R. EphrinB3/EphA4-mediated guidance of ascending and descending spinal tracts. *Neuron.* 2013;80(6):1407-20.
28. Afshari FT, Kwok JC, and Fawcett JW. Astrocyte-produced ephrins inhibit schwann cell migration via VAV2 signaling. *The Journal of neuroscience : the official journal of the Society for Neuroscience.* 2010;30(12):4246-55.
29. Parrinello S, Napoli I, Ribeiro S, Wingfield Digby P, Fedorova M, Parkinson DB, Doddrell RD, Nakayama M, Adams RH, and Lloyd AC. EphB signaling directs peripheral nerve regeneration through Sox2-dependent Schwann cell sorting. *Cell.* 2010;143(1):145-55.
30. Arvanitis DN, Behar A, Tryoen-Toth P, Bush JO, Jungas T, Vitale N, and Davy A. Ephrin B1 maintains apical adhesion of neural progenitors. *Development.* 2013;140(10):2082-92.
31. Davy A, and Robbins SM. Ephrin-A5 modulates cell adhesion and morphology in an integrin-dependent manner. *The EMBO journal.* 2000;19(20):5396-405.
32. Yu M, Wang J, Muller DJ, and Helenius J. In PC3 prostate cancer cells ephrin receptors crosstalk to beta1-integrins to strengthen adhesion to collagen type I. *Scientific reports.* 2015;5(8206.
33. Santiago A, and Erickson CA. Ephrin-B ligands play a dual role in the control of neural crest cell migration. *Development.* 2002;129(15):3621-32.
34. Maro GS, Vermeren M, Voiculescu O, Melton L, Cohen J, Charnay P, and Topilko P. Neural crest boundary cap cells constitute a source of neuronal and glial cells of the PNS. *Nature neuroscience.* 2004;7(9):930-8.
35. Bachelin C, Lachapelle F, Girard C, Moissonnier P, Serguera-Lagache C, Mallet J, Fontaine D, Chojnowski A, Le Guern E, Nait-Oumesmar B, et al. Efficient myelin repair in the macaque

bioRxiv preprint doi: https://doi.org/10.1101/498261; this version posted December 16, 2018. The copyright holder for this preprint (which was not certified by peer review) is the author/funder, who has granted bioRxiv a license to display the preprint in perpetuity. It is made available under aCC-BY-NC-ND 4.0 International license.

spinal cord by autologous grafts of Schwann cells. *Brain : a journal of neurology.* 2005;128(Pt 3):540-9.

36. Girolamo F, Coppola C, Ribatti D, and Trojano M. Angiogenesis in multiple sclerosis and experimental autoimmune encephalomyelitis. *Acta neuropathologica communications.* 2014;2(84.
37. Zujovic V, Thibaud J, Bachelin C, Vidal M, Coulpier F, Charnay P, Topilko P, and Baron-Van Evercooren A. Boundary cap cells are highly competitive for CNS remyelination: fast migration and efficient differentiation in PNS and CNS myelin-forming cells. *Stem cells.* 2010;28(3):470-9.
38. Woodhoo A, Sahni V, Gilson J, Setzu A, Franklin RJ, Blakemore WF, Mirsky R, and Jessen KR. Schwann cell precursors: a favourable cell for myelin repair in the Central Nervous System. *Brain : a journal of neurology.* 2007;130(Pt 8):2175-85.
39. Le N, Nagarajan R, Wang JY, Araki T, Schmidt RE, and Milbrandt J. Analysis of congenital hypomyelinating Egr2Lo/Lo nerves identifies Sox2 as an inhibitor of Schwann cell differentiation and myelination. *Proceedings of the National Academy of Sciences of the United States of America.* 2005;102(7):2596-601.
40. Topilko P, Schneider-Maunoury S, Levi G, Baron-Van Evercooren A, Chennoufi AB, Seitanidou T, Babinet C, and Charnay P. Krox-20 controls myelination in the peripheral nervous system. *Nature.* 1994;371(6500):796-9.
41. Taylor H, Campbell J, and Nobes CD. Ephs and ephrins. *Current biology : CB.* 2017;27(3):R90-R5.
42. Lisabeth EM, Falivelli G, and Pasquale EB. Eph receptor signaling and ephrins. *Cold Spring Harb Perspect Biol.* 2013;5(9).
43. Freywald A, Sharfe N, and Roifman CM. The kinase-null EphB6 receptor undergoes transphosphorylation in a complex with EphB1. *The Journal of biological chemistry.* 2002;277(6):3823-8.
44. Royet A, Broutier L, Coissieux MM, Malleval C, Gadot N, Maillet D, Gratadou-Hupon L, Bernet A, Nony P, Treilleux I, et al. Ephrin-B3 supports glioblastoma growth by inhibiting apoptosis induced by the dependence receptor EphA4. *Oncotarget.* 2017;8(14):23750-9.
45. Nievergall E, Lackmann M, and Janes PW. Eph-dependent cell-cell adhesion and segregation in development and cancer. *Cellular and molecular life sciences : CMLS.* 2012;69(11):1813-42.
46. Lefcort F, Venstrom K, McDonald JA, and Reichardt LF. Regulation of expression of fibronectin and its receptor, alpha 5 beta 1, during development and regeneration of peripheral nerve. *Development.* 1992;116(3):767-82.
47. Jones NP, Peak J, Brader S, Eccles SA, and Katan M. PLCgamma1 is essential for early events in integrin signalling required for cell motility. *Journal of cell science.* 2005;118(Pt 12):2695-706.
48. Akassoglou K, Akpinar P, Murray S, and Strickland S. Fibrin is a regulator of Schwann cell migration after sciatic nerve injury in mice. *Neuroscience letters.* 2003;338(3):185-8.
49. Glebova NO, and Ginty DD. Growth and survival signals controlling sympathetic nervous system development. *Annu Rev Neurosci.* 2005;28(191-222.
50. Park JA, Choi KS, Kim SY, and Kim KW. Coordinated interaction of the vascular and nervous systems: from molecule- to cell-based approaches. *Biochemical and biophysical research communications.* 2003;311(2):247-53.
51. del Zoppo GJ. Inflammation and the neurovascular unit in the setting of focal cerebral ischemia. *Neuroscience.* 2009;158(3):972-82.
52. Li S, Haigh K, Haigh JJ, and Vasudevan A. Endothelial VEGF sculpts cortical cytoarchitecture. *The Journal of neuroscience : the official journal of the Society for Neuroscience.* 2013;33(37):14809-15.
53. Gupta R, Gray M, Chao T, Bear D, Modafferi E, and Mozaffar T. Schwann cells upregulate vascular endothelial growth factor secondary to chronic nerve compression injury. *Muscle & nerve.* 2005;31(4):452-60.

bioRxiv preprint doi: https://doi.org/10.1101/498261; this version posted December 16, 2018. The copyright holder for this preprint (which was not certified by peer review) is the author/funder, who has granted bioRxiv a license to display the preprint in perpetuity. It is made available under aCC-BY-NC-ND 4.0 International license.

54. Greenberg DA, and Jin K. From angiogenesis to neuropathology. *Nature.* 2005;438(7070):954-9.
55. Lu P, Takai K, Weaver VM, and Werb Z. Extracellular matrix degradation and remodeling in development and disease. *Cold Spring Harbor perspectives in biology.* 2011;3(12).
56. Boroujerdi A, Welser-Alves JV, and Milner R. Extensive vascular remodeling in the spinal cord of pre-symptomatic experimental autoimmune encephalomyelitis mice; increased vessel expression of fibronectin and the alpha5beta1 integrin. *Exp Neurol.* 2013;250(43-51.
57. Stoffels JM, Zhao C, and Baron W. Fibronectin in tissue regeneration: timely disassembly of the scaffold is necessary to complete the build. *Cellular and molecular life sciences : CMLS.* 2013;70(22):4243-53.
58. Baron-Van Evercooren A, Duhamel-Clerin E, Boutry JM, Hauw JJ, and Gumpel M. Pathways of migration of transplanted Schwann cells in the demyelinated mouse spinal cord. *J Neurosci Res.* 1993;35(4):428-38.
59. Kotter MR, Li WW, Zhao C, and Franklin RJ. Myelin impairs CNS remyelination by inhibiting oligodendrocyte precursor cell differentiation. *The Journal of neuroscience : the official journal of the Society for Neuroscience.* 2006;26(1):328-32.
60. Krikorian D, Manthorpe M, and Varon S. Purified mouse Schwann cells: mitogenic effects of fetal calf serum and fibroblast growth factor. *Developmental neuroscience.* 1982;5(1):77-91.
61. Bottenstein JE, and Sato GH. Fibronectin and polylysine requirement for proliferation of neuroblastoma cells in defined medium. *Exp Cell Res.* 1980;129(2):361-6.
62. Renier N, Wu Z, Simon DJ, Yang J, Ariel P, and Tessier-Lavigne M. iDISCO: a simple, rapid method to immunolabel large tissue samples for volume imaging. *Cell.* 2014;159(4):896-910.
63. Jourdren L, Bernard M, Dillies MA, and Le Crom S. Eoulsan: a cloud computing-based framework facilitating high throughput sequencing analyses. *Bioinformatics.* 2012;28(11):1542-3.
64. Dobin A, Davis CA, Schlesinger F, Drenkow J, Zaleski C, Jha S, Batut P, Chaisson M, and Gingeras TR. STAR: ultrafast universal RNA-seq aligner. *Bioinformatics.* 2013;29(1):15-21.
65. Li H, Handsaker B, Wysoker A, Fennell T, Ruan J, Homer N, Marth G, Abecasis G, Durbin R, and Genome Project Data Processing S. The Sequence Alignment/Map format and SAMtools. *Bioinformatics.* 2009;25(16):2078-9.
66. Anders S, Pyl PT, and Huber W. HTSeq--a Python framework to work with high-throughput sequencing data. *Bioinformatics.* 2015;31(2):166-9.
67. Anders S, and Huber W. Differential expression analysis for sequence count data. *Genome biology.* 2010;11(10):R106.
68. Norton WT, and Poduslo SE. Myelination in rat brain: method of myelin isolation. *Journal of neurochemistry.* 1973;21(4):749-57.
69. Davis S, Gale NW, Aldrich TH, Maisonpierre PC, Lhotak V, Pawson T, Goldfarb M, and Yancopoulos GD. Ligands for EPH-related receptor tyrosine kinases that require membrane attachment or clustering for activity. *Science.* 1994;266(5186):816-9.
70. Fan XY, Mothe AJ, and Tator CH. Ephrin-B3 decreases the survival of adult rat spinal cord-derived neural stem/progenitor cells in vitro and after transplantation into the injured rat spinal cord. *Stem cells and development.* 2013;22(3):359-73.
71. Bachelin C, Zujovic V, Buchet D, Mallet J, and Baron-Van Evercooren A. Ectopic expression of polysialylated neural cell adhesion molecule in adult macaque Schwann cells promotes their migration and remyelination potential in the central nervous system. *Brain : a journal of neurology.* 2010;133(Pt 2):406-20.

Figure 1

bioRxiv preprint doi: https://doi.org/10.1101/498261; this version posted December 16, 2018. The copyright holder for this preprint (which was not certified by peer review) is the author/funder, who has granted bioRxiv a license to display the preprint in perpetuity. It is made available under aCC-BY-NC-ND 4.0 International license.

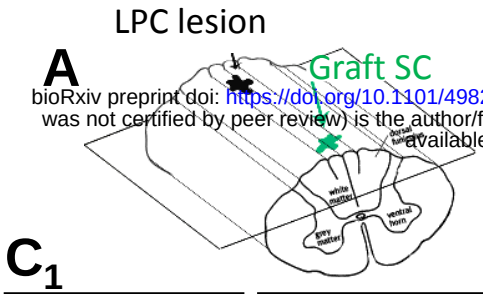

B	Distance graft-LPC injections (mm)	Distance SC towards lesion (mm)	Animals with SC within the lesion
1dpi	4.3±0.44	1.06±0.48	0%
3dpi	4.5±0.44	2.75±0.88	28%
5dpi	4.1±0.69	4.57±0.79	100%

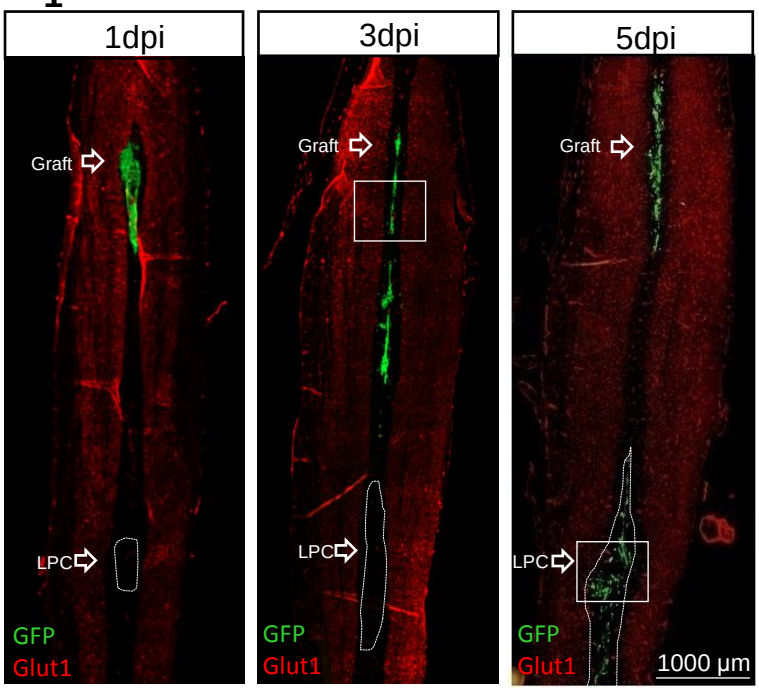

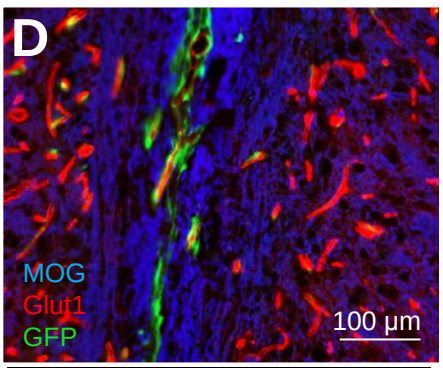

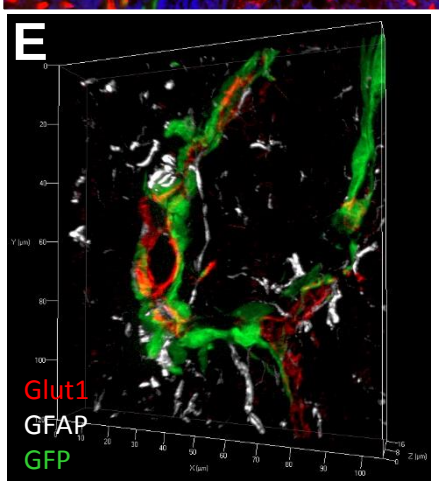

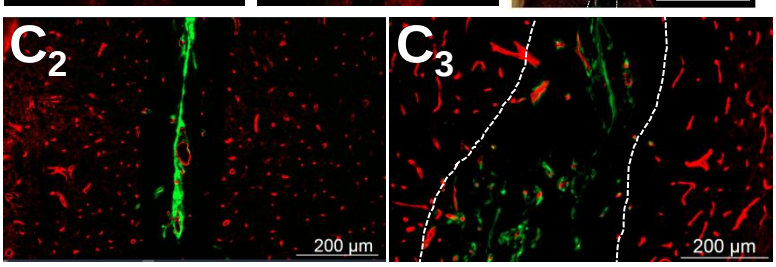

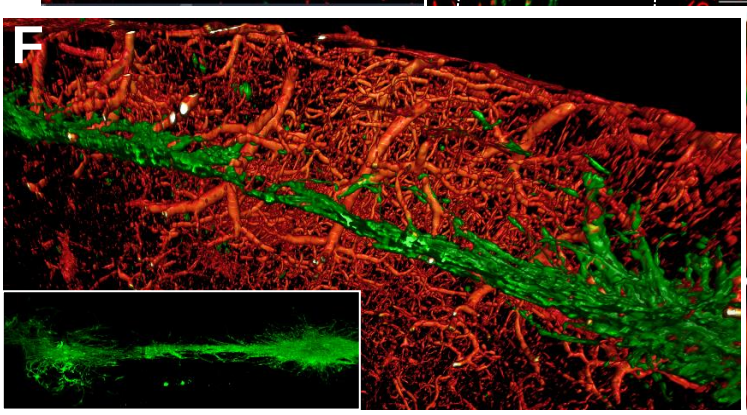

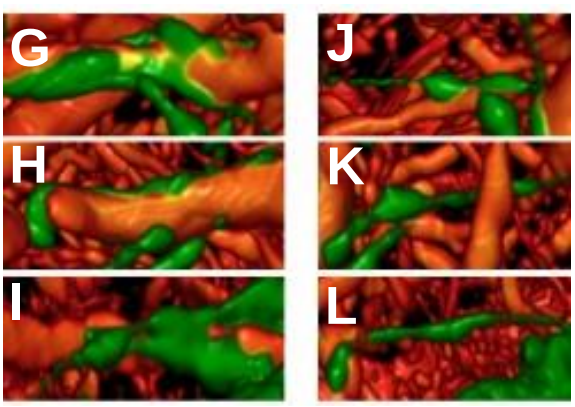

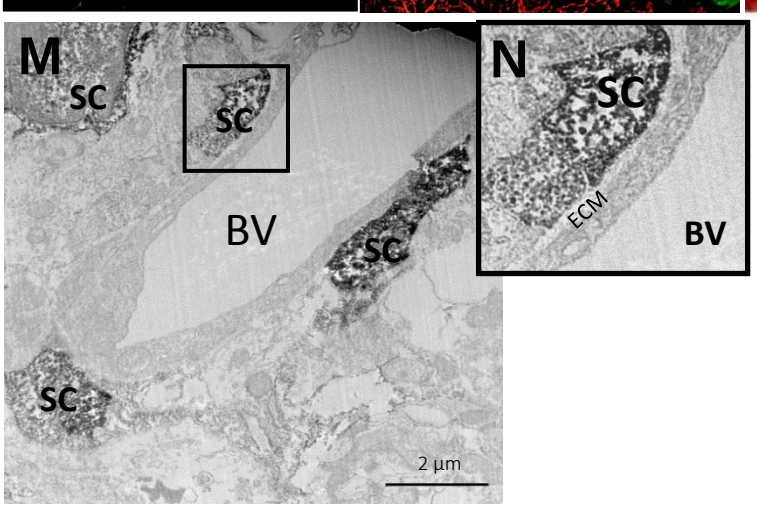

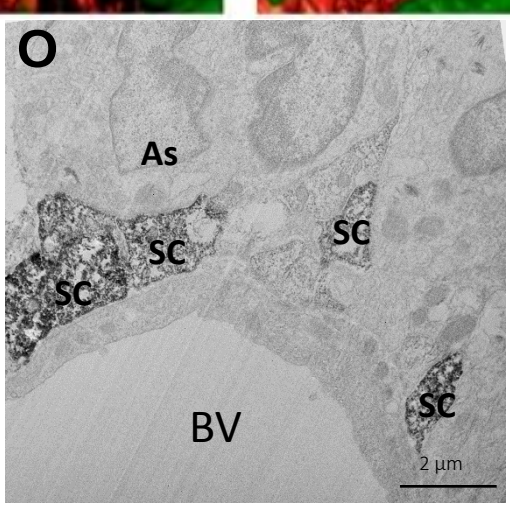

bioRxiv preprint doi: https://doi.org/10.1101/498261; this version posted December 16, 2018. The copyright holder for this preprint (which was not certified by peer review) is the author/funder, who has granted bioRxiv a license to display the preprint in perpetuity. It is made available under aCC-BY-NC-ND 4.0 International license.

Fig. 1. Migrating behavior of SC grafted in white matter remotely from LPC-induced demyelination.

(A) Scheme of LPC lesion and SC graft targeted into the dorsal funiculus of the spinal cord, graft and lesion are 4mm apart. (B) Quantification of SC distance of migration and recruitment by the lesion. Extent of migration and percentage of animals with lesions containing SC at different times, shows that the SC arrival at the lesion is timely regulated. Data are expressed as mean ± SD, 1dpi (n=5), 3dpi (n=6), 5dpi (n=7). (C_1) General view of longitudinal sections of the spinal cord illustrating the graft and lesion sites at 1dpi, 3dpi and 5dpi, stained for Glut1. GFP^+SC grafted within dorsal spinal cord white matter progress along the midline, migrate preferentially in close contact with $Glut1^+$ endothelial cells towards the lesion (C_2) and spread within the lesion close to the BV (C_3). Dotted lines identify the graft and lesion sites. (D) Grafted GFP^+SC along the midline in the intermediate zone avoid myelin (revealed with MOG) and are associated with $Glut1^+$BV. (E) 3D reconstruction from a Z stack illustrating GFP^+SC located between $Glut1^+$endothelial cells and perivascular astroglial end feet ($GFAP^+$). (F) 3D reconstruction after light sheet imaging of clarified whole spinal cord illustrates the abundant vascular spinal cord network and $tdTomato^+$SC migrating from the graft along the dorsal funiculus midline (intermediate zone) en route for the lesion. While a few of $tdTomato^+$SC escape from the graft in other directions, most $tdTomato^+$SC exiting the graft are polarized on BV (G,H,I) or between BV evoking jumping events from one BV to another one (J,K,L). Immuno-EM of GFP^+SC in the intermediate zone illustrates several GFP^+SC revealed by DAB embedded in perivascular ECM (M) between BV and astrocytes (As) (O). (N) Higher magnification of the boxed area in (M).

Figure 2

bioRxiv preprint doi: https://doi.org/10.1101/498261 ... posted December 18, 2018. The copyright holder for this preprint (which was not certified by peer review) is the author/funder, who has granted bioRxiv a license to display the preprint in perpetuity. It is made available under CC-BY-NC-ND 4.0 International license.

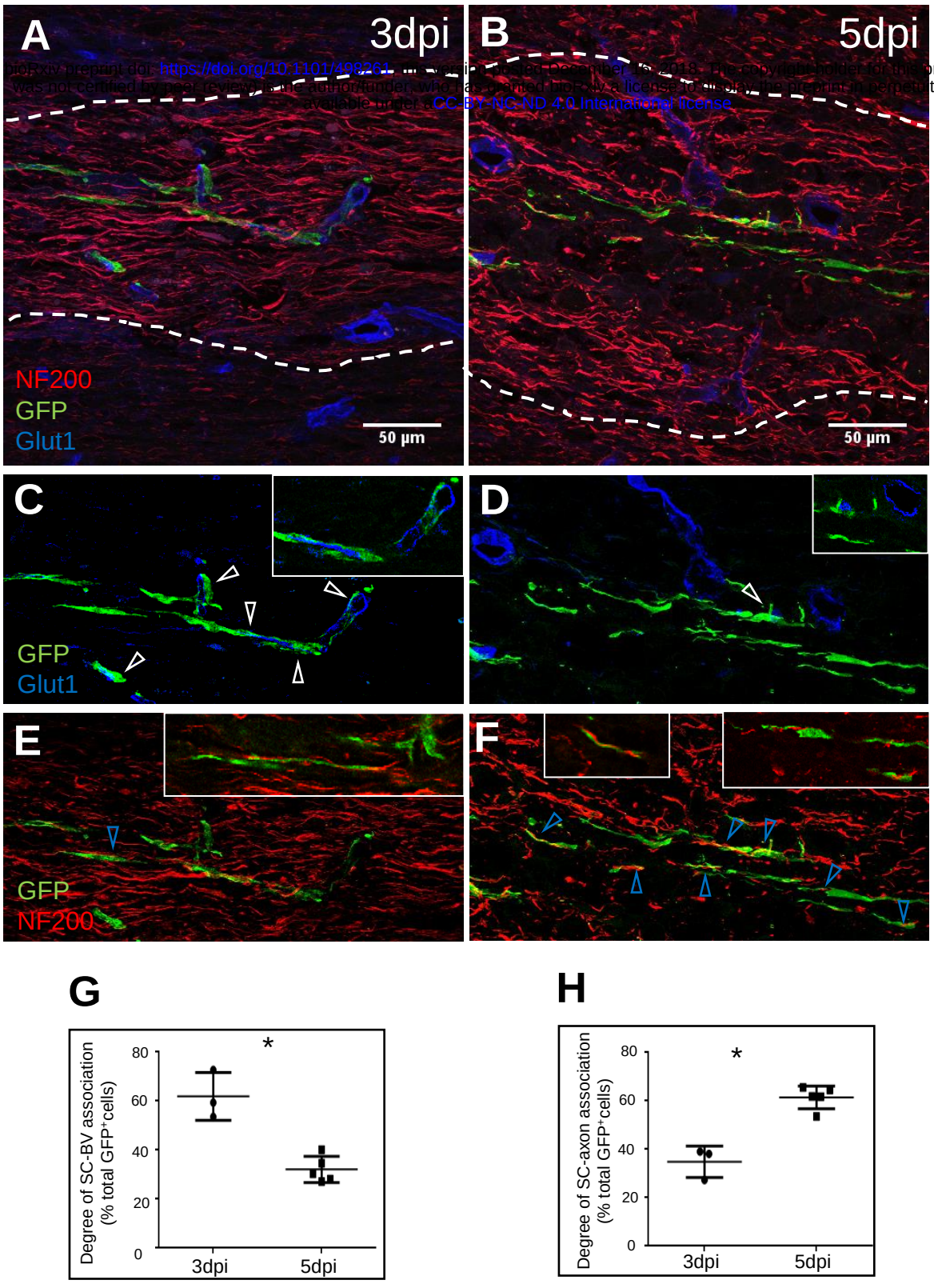

Fig. 2. Schwann cells migrate along BV and timely dissociate from them to contact demyelinated axons at the lesion site. (A,C,E) Upon arrival at the lesion at 3dpi, grafted GFP$^+$SC are associated with BV. (B,D,F) At 5dpi, fewer SC are associated with BV but are aligned with NF200$^+$axons. (C,D) Higher magnifications of GFP$^+$ cells in the lesion illustratinghe temporal decrease of association of GFP$^+$SC with Glut1-positive BV (white arrows) compared to(E-F) the progressive increase of GFP$^+$SC in association with NF200$^+$ axons (blue arrow). (G,H) Quantification of SC associated or not, with BV at 3dpi (n=2) and 5dpi (n=8) (two-tailed Mann Whitney test p=0.035) (the experiments were repeated independently three times, mean value ± SD). C, E and D, F show separated colors of A and B respectively. A-F images represent confocal maximal projections of Z-stacks, while insets show only one confocal Z-plane.

Figure 3

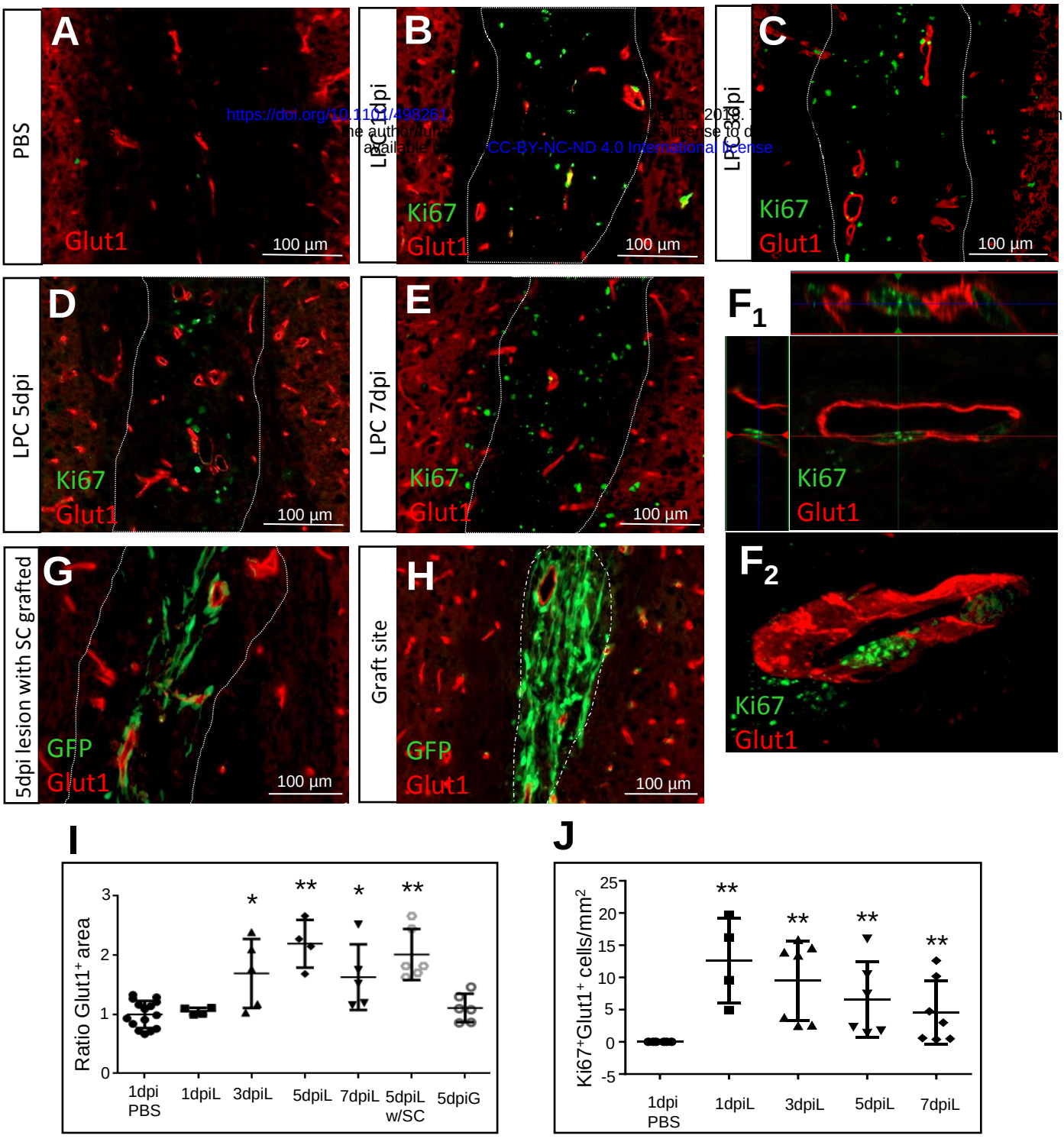

https://doi.org/10.1101/498261 ... CC-BY-NC-ND 4.0 International license

Fig. 3. Dynamics of the vascular network in response to LPC demyelination. Immunohistochemistry for Glut1$^+$ (red) at 1dpi (B), 3dpi (C), 5dpi (D) and 7dpi (E) illustrates increased vascularization in LPC lesions compared to control (A). (F_1) Orthogonal and (F_2) 3D views show proliferating Glu1$^+$Ki67$^+$ endothelial cells. (G,H) Immunohistochemistry for Glut1$^+$ at lesion site (G) and graft site (H) in SC grafted mice at 5dpi. (I) Quantification of Glut1$^+$area shows a significant expansion of BV from 3dpi-7dpi, with a peak at 5dpi, which is similar to that observed in lesions of grafted animals. Glut1$^+$ quantification showed no increase in Glut1$^+$ area at the graft site. (Glut1$^+$area in Lesion/PBS (n=15): 1dpi (n=4): 1±0.05; 3dpi (n=4): 1.8±0.5; 5dpi (n=4): 2.2±0.4; and 7dpi (n=7): 1.6±0.5; 5dpi in lesion of grafted mice/PBS (n=6): 2±0.4; 5dpi in SC graft site (n=6): 1.1±0.2; one-way ANOVA p<0.001, F(4,28)=10.96; two-tailed Mann Whitney test with PBS group: 3dpi (p=0.019); 5dpi (p=0.0005); and 7dpi (p=0.01). Values are expressed as the ratio to the PBS mean). (J) The number of Glut1$^+$/Ki67$^+$ cells increases at 1dpi preceding that Glut1$^+$area, and declining thereafter (1dpi (n=4): 12.7±7 (p=0.004), 3dpi (n=4): 7.8±7 (p=0.001), 5dpi (n=4): 6.5±6 (p=0.002), 7dpi (n=7): 2.9±4 (p=0.001); one-way ANOVA p=0.007, F(4,25)=4.48; two-tailed Mann Whitney test with PBS group: 1dpi (p=0.004), 3dpi (p=0.001), 5dpi (p=0.002), 7dpi (p=0.001). Dashed lines highlight the lesion border defined by GFAP immunostaining and Hoechst hyper-cellularity, and graft site. Data are expressed as mean value ± SD of control (PBS). The experiments were repeated independently three times. **means p<0.01 and *means p<0.05.

Figure 4

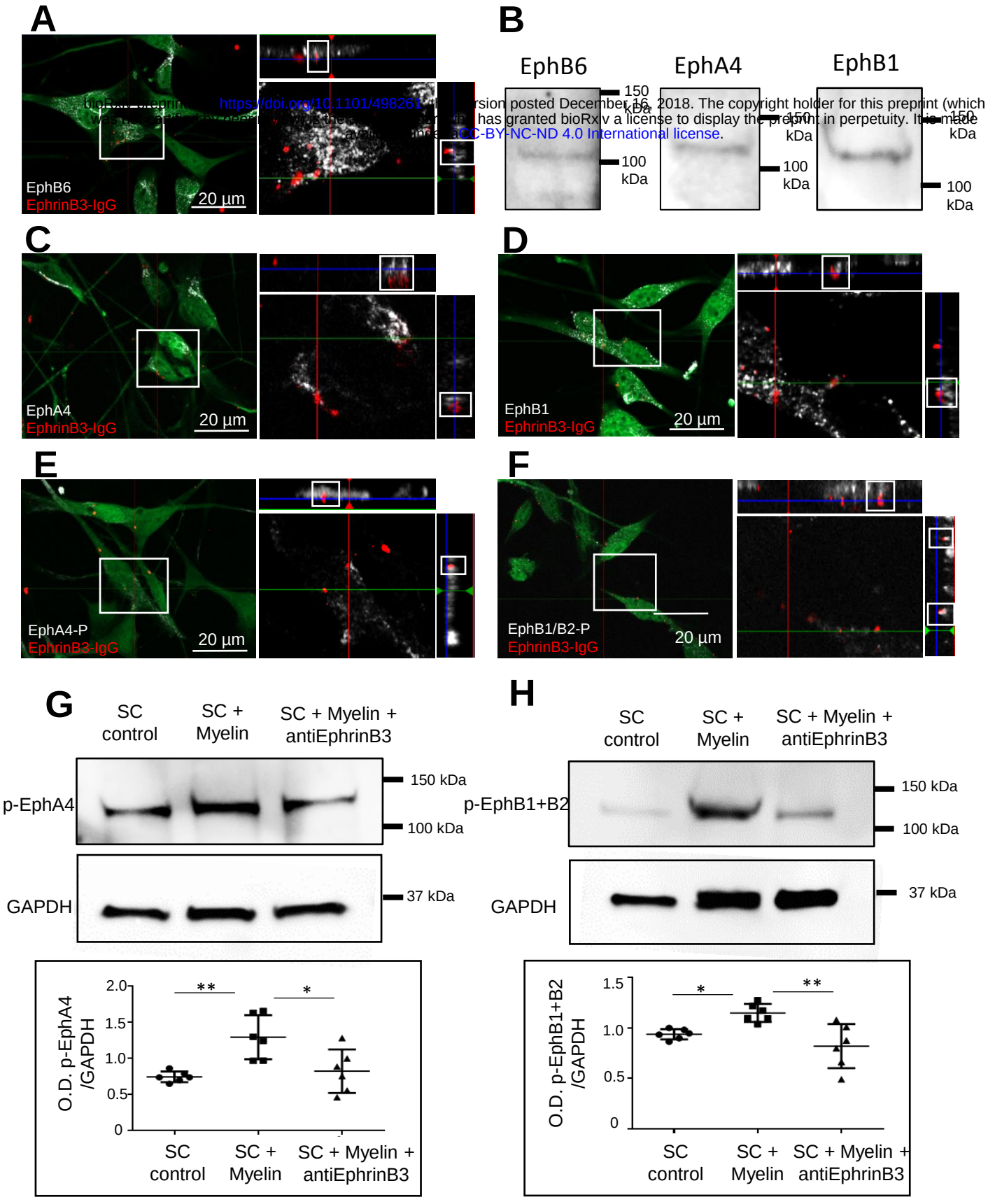

https://doi.org/10.1101/498261 ... version posted December 16, 2018. The copyright holder for this preprint (which ... has granted bioRxiv a license to display the preprint in perpetuity. It is made ... CC-BY-NC-ND 4.0 International license.

Fig 4. EphrinB3 binds and activates EphA4, EphB1 and EphB6 receptors in SC. (A, C, D) Orthogonal views of SC activation with clustered-EphrinB3 shows that EphrinB3 binds EphB6 (A), EphA4 (C) and EphB1 (D) receptors on SC. (B) Western blot analysis confirmed the presence of these receptors in SC. (E,F) Bound EphrinB3 activation of EphA4 and EphB receptors viewed by immunodetection of phosphorylated forms. (G,H) SC incubation with myelin increased the phosphorylation of EphA4 (G) and EphB1+B2 (H) by Western blotting, which is not the case when myelin is previously blocked by anti-EphrinB3 antibody (O.D. of p-EphB1+2/GAPDH control (n=6): 0.93±0.05, myelin (n=6): 1.1±0.08, myelin+anti-EphrinB3 (n=6): 0.82±0.21) (one-way ANOVA p=0.003, F(2,15)=8.57, followed by a Tukey's multiple comparison test); and O.D. of p-EphA4/GAPDH control (n=6): 0.74±0.07, myelin (n=6): 1.29±0.30, myelin+anti-EphrinB3 (n=6): 0.82±0.30 (one-way ANOVA p=0.0036, F(2,15)=8.44, followed by a Tukey's multiple comparison test). Quantification was assessed in at least 3 independent experiments and data are expressed as ratio of the optical density (O.D.) of the bands (mean values ± SD).

Figure 5

bioRxiv preprint doi: https://doi.org/10.1101/498261; this version posted December 16, 2018. The copyright holder for this preprint (which was not certified by peer review) is the author/funder, who has granted bioRxiv a license to display the preprint in perpetuity. It is made available under aCC-BY-NC-ND 4.0 International license.

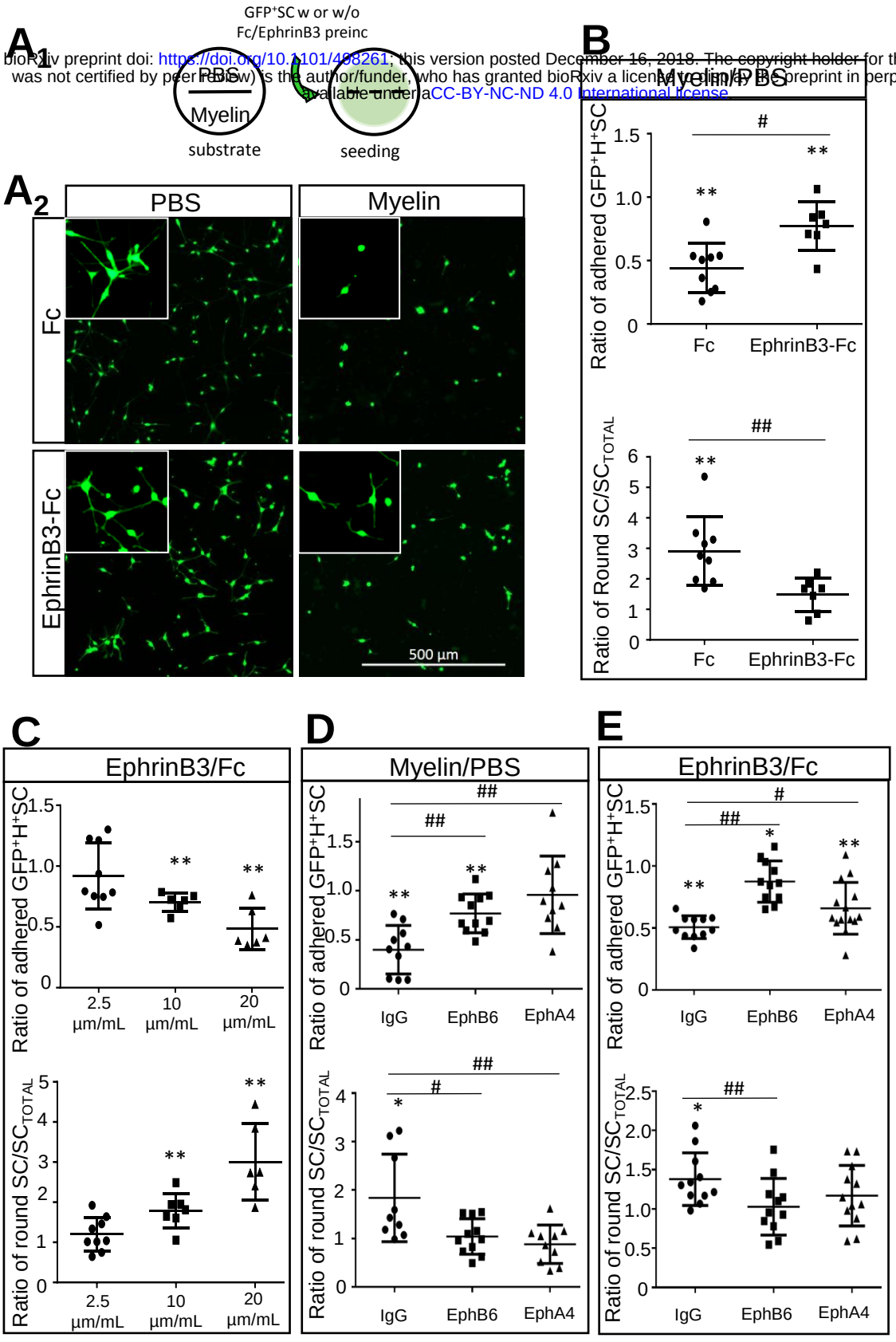

bioRxiv preprint doi: https://doi.org/10.1101/498261; this version posted December 16, 2018. The copyright holder for this preprint (which was not certified by peer-review) is the author/funder, who has granted bioRxiv a license to display the preprint in perpetuity. It is made available under aCC-BY-NC-ND 4.0 International license.

Fig 5. EphrinB3 mediates myelin-inhibition on SC adhesion and polarization through EphA4 and EphB6 receptors. (A_1) Diagram of the adhesion assay. Coverslips divided by silicon strips were coated with PBS (non-coated control) or myelin in each half. After removing the strip, cells pre-incubated with Fc or EphrinB3 were seeded homogenously on the coverslip. (A_2) Unclustered EphrinB3 partially reverts myelin-induced inhibition of SC adhesion and spreading. (B) Quantification of the number of adhered and polarized GFP^+SC. Pre-incubation of SC with unclustered EphrinB3 promotes their adhesion and spreading on myelin-coated surfaces compared to those pre-incubated with Fc only. Ratio of adhered cells Myelin/PBS; Fc-preincubated SC on myelin(n=9): 0.4±0.2 (**p<0.0001); EphrinB3-preincubated SC on myelin(n=7): 0.8±0.2 (**p=0.0009); #p=0.01. Ratio of round cells Myelin/PBS: Fc(n=9): 2.9±1 (**p=0.0009); EphrinB3(n=7): 1.5±0.5, ##p=0.0021. (C) SC seeded on substrate coated with increased concentrations of EphrinB3, adhere and spread less in a dose concentration manner respect to the intra-coverslip control (Fc) substrate. Ratio of adhered cells EphrinB3/Fc; 2.5µg/mL(n=9): 0.9±0.3, 10µg/mL(n=7): 0.7±0.07 (**p=0.002) and 20µg/mL(n=6): 0.5±0.2 (**p=0.007), one-way ANOVA (p=0.003, F(2,18)=8.21). Ratio of round cells EphrinB3/Fc: 2.5µg/mL(n=9): 1.2±0.4, 10µg/mL(n=7): 1.8±0.4 (**p=0.003) and 20ug/mL(n=6): 3±0.9 (**p=0.003), one-way ANOVA (p<0.001, F(2,19)=15.81).(D, E) Quantification of the number of adhered and polarized SC pre-incubated with anti-EphB6 or anti-EphA4 (extracellular domain). Pre-incubation with anti-EpB6 and anti-EphA4 improves the number of adhered and polarized SC on Myelin (D) and EphrinB3 (E) compared to PBS and Fc respectively. Pre-incubation with IgG as control shows similar results than non-preincubated cells (B, C). Ratio of adhered cells Myelin/PBS: IgG(n=10): 0.4±0.2 (*p<0.0001); anti-EphB6(n=11): 0.9±0.4, anti-EphA4(n=9): 0.8±0.2; one-way ANOVA p<0.001, F(2,27)=10.21; ##*p*(IgG vs anti-EphB6)=0.001; ##*p*(IgG vs anti-EphA4)=0.001. Ratio of adhered cells EphrinB3/Fc: IgG(n=11): 0.5±0.09 (*p<0.0001), anti-EphB6(n=11): 0.9±0.2, anti-EphA4(n=14): 0.6±0.2; ANOVA p<0.001, F(2,33)=13.42; #*p*(IgG vs anti-EphA4)=0.03; ##*p*(IgG vs anti-EphB6)=0.0001. Ratio of round cells Myelin/PBS: IgG(n=9): 1.8±0.9 (*p=0.02), anti-EphB6(n=11): 1.0±0.4, anti-EphA4(n=10): 0.8±0.4, one-way ANOVA p=0.003, F(2,27)=7.17; #*p*(IgG vs anti-EphB6)=0.01; ##*p*(IgG vs anti-EphA4)=0.007. Ratio of round cells EphirnB3/Fc: IgG(n=11): 1.4±0.3 (**p=0.003), anti-EphB6(n=11): 1.0±0.4, anti-EphA4(n=12): 1.2±0.4, one-way ANOVA p=0.08, F(2,31)=2.65; #*p*(IgG vs anti-EphB6)=0.02; ##*p*(IgG vs anti-EphA4)=0.17. Data are expressed as ratio (mean values ± SD) of Myelin or EphrinB3 surfaces compared to intra-coverslips control non-coated surfaces (PBS) or with equimolar concentration of Fc respectively. */** are used for comparison of a group with its hypothetical mean: 1 by one sample two-tailed t-test, and #/## for comparison between two different groups by two-tailed Mann Whitney test. *means p<0.05; **means p<0.01; #means p<0.05; ##means p<0.001.

Figure 6

bioRxiv preprint doi: https://doi.org/10.1101/498261; this version posted December 16, 2018. The copyright holder for this preprint (which was not certified by peer review) is the author/funder, who has granted bioRxiv a license to display the preprint in perpetuity. It is made available under aCC-BY-NC-ND 4.0 International license.

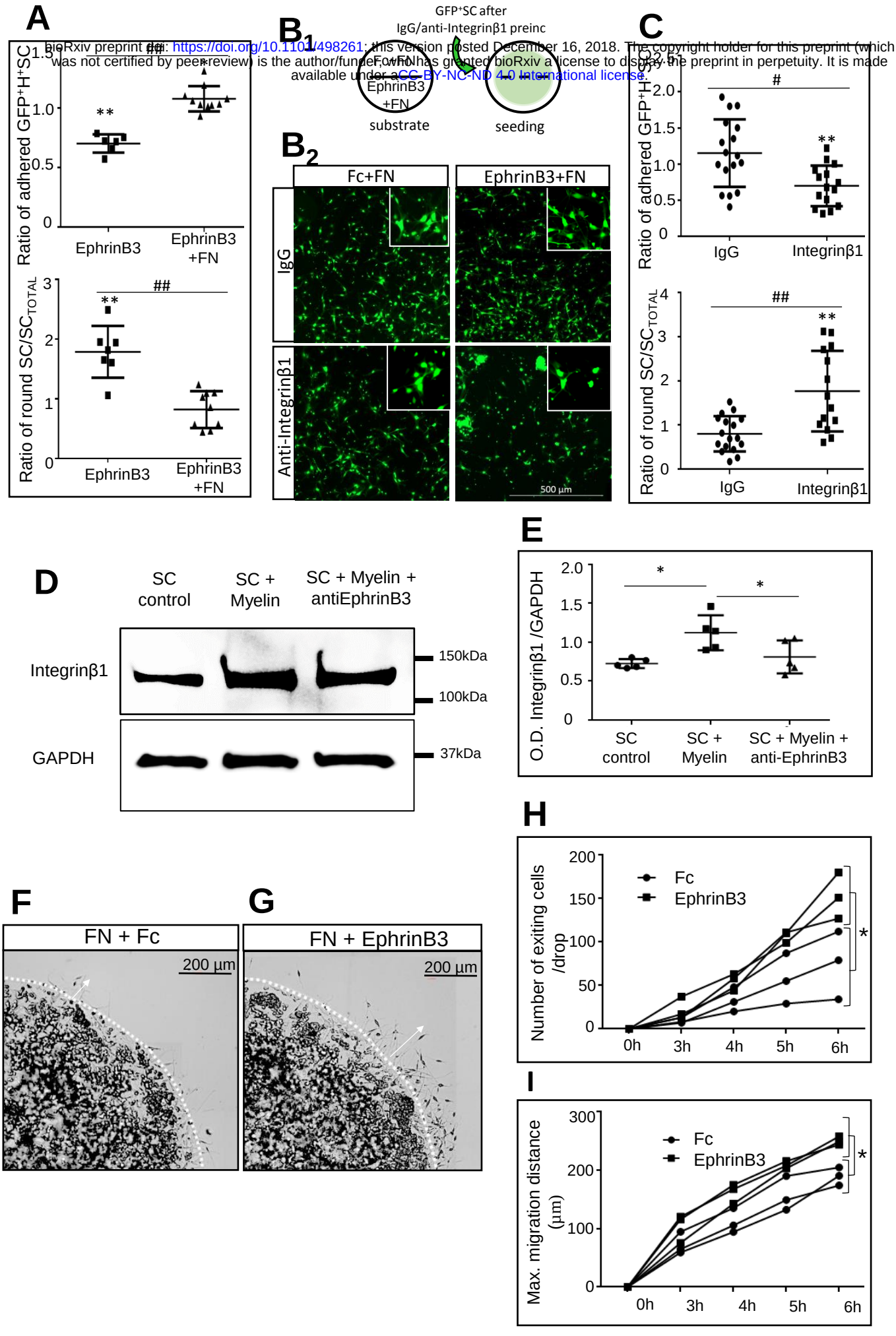

bioRxiv preprint doi: https://doi.org/10.1101/498261; this version posted December 16, 2018. The copyright holder for this preprint (which was not certified by peer review) is the author/funder, who has granted bioRxiv a license to display the preprint in perpetuity. It is made available under aCC-BY-NC-ND 4.0 International license.

Fig 6. EphrinB3 improves SC adhesion and migration on FN coated surfaces. (A) Quantification of the number of adhered and polarized SC seeded on substrate coated with EphrinB3 with or without FN. Data are expressed as ratio (mean values ± SD) respect to Fc-non FN coated surfaces. Ratio of adhered cells: EphrinB3 (10µg/mL) (n=7): 0.7±0.07 (**p=0.002), EphrinB3 (10µg/mL) + FN (2µg/cm^2) (n=10): 1.07±0.1 (*p=0.04); ##p(FN+EphrinB3 vs FN=Fc)=0.001. Ratio of round cells: EphrinB3 (10µg/mL) (n=7): 1.8±0.4 (**p=0.003), EphrinB3 (10µg/mL) + FN (2µg/cm^2) (n=10): 0.82±0.3 (p=0.11); ##p(FN+EphrinB3 vs FN=Fc)<0.001. **.** (B_1) Diagram of the adhesion assay on FN. Coverslips divided by silicon strips were coated with Fc+FN (control) or EphrinB3+FN in each half. After strip removal, cells pre-incubated with IgG or anti-Integrinβ1 were seeded homogenously on the coverslip. (B_2) Blocking Integrinβ1 decreases SC adhesion and polarization to substrates coated with EphrinB3+FN compared to those coated with Fc+FN. (C) Quantification of SC adhesion and polarization on EphrinB3 when SC are pre-incubated with IgG or anti-integrinß1. Data are expressed as ratio (mean values ± SD) over control (Fc+FN substrate); IgG (n=17): 1.1±0.4; anti-integrinβ1 (n=15): 0.7±0.3; #p=0.01. (D) Western blot analysis shows increased expression of Integrinβ1 when SC are activated by myelin extracts.(E) This increase is not significant when myelin is incubated with anti-EphrinB3 before the assay. (D,E) O.D. of Integrin β1/GAPDH control (n=5): 0.72±0.05, myelin (n=5): 1.12±0.22, myelin+anti-EphrinB3 (n=5): 0.81±0.21; one-way ANOVA p=0.011, F(2,12)=6.62;, followed by Tukey's multiple comparisons test. (F,G). Exit of SC entrapped in an agarose drop and seeded on FN + Fc (F) and FN+EphrinB3 (Fc: n=3, EphrinB3: n=3). (H) More SC exit from the agarose drop after 5h post-seeding (two-way ANOVA with repeated measures p=0.03, F(1,4)=10.24) and (I) migrate over longer distances from the drop-edge from 4h on (two-way ANOVA with repeated measures p=0.02, F(1,4)=12.74)on combined FN and EphrinB3 coated surfaces. Graphs represent the values of separate experiments. */** are used for comparison of a group with its hypothetical mean: 1 by one sample two-tailed t-test, and #/## for comparison between two different groups by two-tailed Mann Whitney test.* means p<0.05; ** means p<0.001; # means p<0.05; ## means p<0.001.

Figure 7

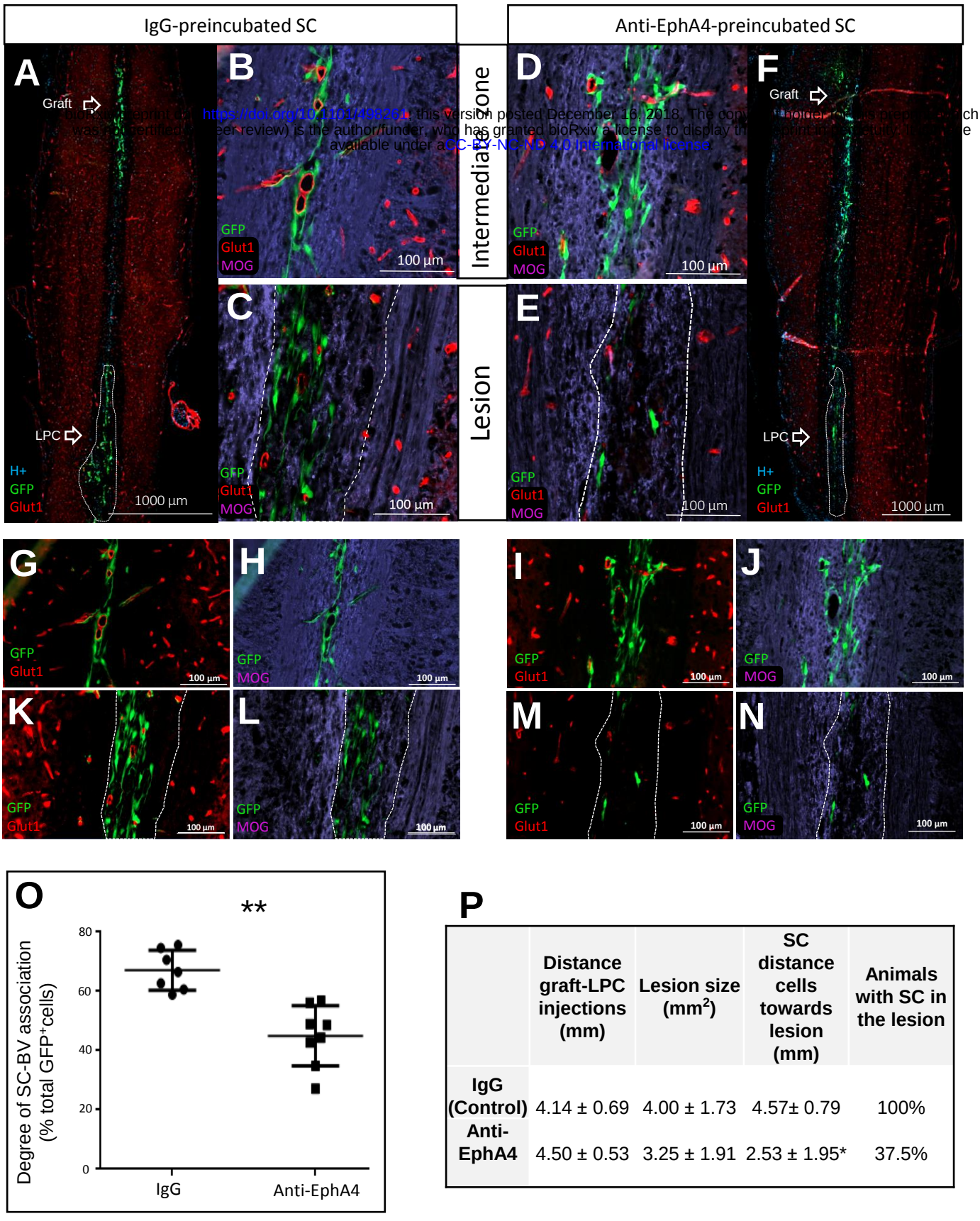

https://doi.org/10.1101/498261 ; this version posted December 16, 2018. The copyright holder for this preprint (which was not certified by peer review) is the author/funder, who has granted bioRxiv a license to display the preprint in perpetuity. It is made available under aCC-BY-NC-ND 4.0 International license.

P

	Distance graft-LPC injections (mm)	Lesion size (mm^2)	SC distance cells towards lesion (mm)	Animals with SC in the lesion
IgG (Control)	4.14 ± 0.69	4.00 ± 1.73	4.57± 0.79	100%
Anti-EphA4	4.50 ± 0.53	3.25 ± 1.91	2.53 ± 1.95*	37.5%

Fig 7. Pre-incubation of SC with anti-EphA4 reduces their migration along BV after transplantation in the demyelinated spinal cord. (A) GFP^+SC pre-incubated with IgG migrate from the graft along the midline in the intermediate zone in association with BV (B,G) but avoid CNS myelin (B,H) before arrival at the lesion at 5dpi (C,K,L). (F) Anti-EphA4-preincubated GFP^+SC exiting the graft mingle more with myelin (D, J), but associate less with BV (D,I) and frequently fail to reach the lesion site at 5dpi (E,M,N). (O) Quantification of SC in association or not, with BV show significant differences between control (IgG) and anti-EphA4 pre-incubated SC with fewer cells associated with BV after anti-EphA4 pre-incubation. (P) Quantification of the extent of migration of grafted GFP^+SC. The reduced extent of migration by SC pre-incubated with anti-EphA4 prior grafting, compared to control SC, correlates with a reduced percentage of animals in which grafted SC are recruited by the lesion. Dashed lines delineate lesions. Data are expressed as mean values ± SD. IgG: n=7, anti-EphA4: n=8; * means $p<0.05$.

Figure 8

bioRxiv preprint doi: https://doi.org/10.1101/498261; this version posted December 16, 2018. The copyright holder for this preprint (which was not certified by peer review) is the author/funder, who has granted bioRxiv a license to display the preprint in perpetuity. It is made available under aCC-BY-NC-ND 4.0 International license.

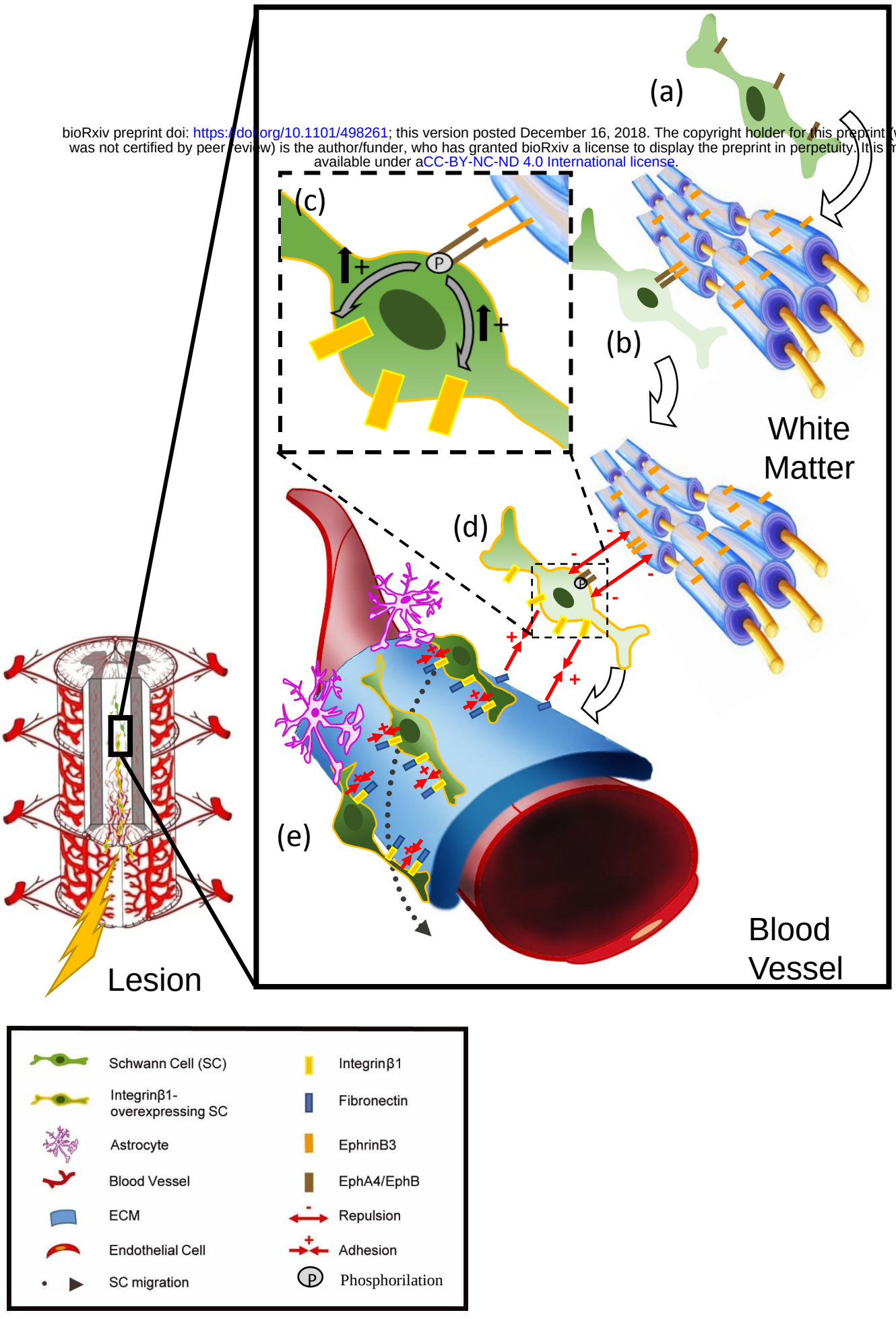

Fig 8. Model of the mechanism of guidance and migration of SC after CNS demyelination. SC invading the CNS (a) are activated by the myelin-associated EphrinB3 through EphB6- and EphA4-SC receptors (b). The activation by phosphorilation of these receptors increases the SC expression of Integrinβ1 (c), impairing the SC adhesion to white matter and promoting their adhesion to BV extracellular matrix (d). In parallel, lesions of white matter undergo the formation and/or remodeling of BV and increases expression of ECM adhesion molecules, in particular FN, which further facilitates SC mobilization towards the lesion (e).